Correspondence to:

S. Ehosioke,
solomon.ehosioke@gmail.com

Spectroscopic Approach Toward Unraveling the Electrical Signature of Roots

Solomon Ehosioke[1,2] [iD], **Sarah Garré[2,3]**, **Johan Alexander Huisman[4]** [iD], **Egon Zimmermann[5]**, **Edmundo Placencia-Gomez[1]** [iD], **Mathieu Javaux[4,6]** [iD], and **Frédéric Nguyen[1]** [iD]

[1]Urban and Environmental Engineering, Liège University, Liège, Belgium, [2]Gembloux Agro-Bio Tech, Liège University, Gembloux, Belgium, [3]Flanders Research Institute for Agriculture, Fisheries and Food, Melle, Belgium, [4]Agrosphere (IBG 3), Forschungszentrum Jülich GmbH, Jülich, Germany, [5]Electronic Systems (ZEA-2), Forschungszentrum Jülich GmbH, Jülich, Germany, [6]Earth and Life Institute, Environmental Science, Université catholique de Louvain, Louvain-la-Neuve, Belgium

Abstract Geoelectrical methods are increasingly used to investigate soil-plant interactions in an agricultural context. For this, it is essential to quantify root electrical properties, since they influence the bulk electrical signal of vegetated soil. This quantification has to be done at the root segment scale with attention for the variability of root properties in time and space as well as within and across plant species. In this study, we investigated the frequency-dependent electrical properties in terms of conduction and polarization of single root segments of Brachypodium (*Brachypodium distachyon* L.) and Maize (*Zea mays* L.). A sample holder to investigate the electrical properties of root segments was designed and tested on ideal resistors. We found that it is suitable to assess the electrical properties of crop root segments of 1–5-cm length in a frequency range between 1 Hz and 45 kHz. The system was then used to obtain the complex electrical response of Brachypodium and Maize root segments at 10 different ages. It was found that the electrical properties of the root segments varied with age and species. This variation was linked to root anatomy based on the microscopic analysis of root sections.

Plain Language Summary Electrical geophysical methods are increasingly used to investigate soil-plant interactions in an agricultural context. For this, it is essential to quantify the electrical properties of roots alone without the soil, since they influence the overall electrical signal of soils in agricultural farms. This quantification has to be done at the root segment scale with attention for the variability of root properties in time and space as well as within and across plant species. In this study, we investigated the frequency-dependent electrical properties of single root segments of Brachypodium and Maize plants. A sample holder to investigate the electrical properties of root segments was designed and tested on ideal resistors. We found that it is suitable to assess the electrical properties of crop root segments of 1–5-cm length in a frequency range between 1 Hz and 45 kHz. The system was then used to obtain the electrical response of Brachypodium and Maize root segments at 10 different ages. It was found that the electrical properties of the root segments varied with age and species. This variation was linked to root anatomy based on the microscopic analysis of root sections.

1. Introduction

Root system architecture, extension, and physiological status play a fundamental role for agriculture and ecosystem productivity. Roots provide water, nutrient, and anchorage to plants by developing into soils or substrates. Under limited resources or adverse environmental conditions, the ability of plant root systems to explore their environment to capture sparsely distributed resources (i.e., plasticity) is crucial for plant development and survival. While the understanding of the genetic and molecular mechanisms for root response to their environment has been improved substantially (Bennett et al., 1996; Marchant et al., 1999; Miyazawa & Takahashi, 2020; Slovak et al., 2016; Su et al., 2017), the characterization of plant root system development in situ (i.e., root phenotyping) is lagging behind due to the inaccessibility of roots and the complexity of root zone processes. Several noninvasive techniques such as magnetic resonance imaging, X-ray computed tomography, and positron emission tomography have been used to investigate root systems in well controlled environments (Atkinson et al., 2019). In field conditions though, there is currently no reliable method to noninvasively investigate root system architecture and its functioning with sufficient accuracy.

Geophysical techniques are increasingly used in agricultural contexts to monitor environmental variables (e.g., soil water content, salinity), soil-root interactions and to help agricultural management (e.g., impact of irrigation and fertilizer application on agricultural production) (Allred et al., 2008). Various studies have used electrical geophysical methods to investigate water dynamics in the root zone (Beff et al., 2013; Garré et al., 2011, 2013; Michot et al., 2003; Srayeddin & Doussan, 2009). Techniques, such as electrical capacitance measurements, electrical resistance measurements, electrical resistivity tomography (ERT), etc., have all been used to investigate root systems in the past decades, as summarized in the reviews of Ehosioke et al. (2020) and Liu et al. (2021). For example, Amato et al. (2008) used ERT to establish a quantitative site-specific relationship between soil electrical resistivity and root biomass of *Alnus glutinosa* trees. Similar correlations were reported for tree roots in a citrus orchard (Rossi et al., 2011) and coffee roots (Paglis, 2013). However, these methods do not yet allow to characterize root functioning or to measure different root traits like angles, root ages, or root hydraulic conductivity, which play a major role in resource acquisition (e.g., Barrowclough et al., 2000; Lynch, 1995; Meunier et al., 2018). It is also not yet known how electrical properties of individual root segments are related to these root traits and how their combination results in the electrical signature of the whole root system. A better understanding of the electrical signature of roots is therefore important not only to improve the information content and reduce inaccuracy of electrical measurements in soil in general but also to obtain insights in root properties noninvasively.

Spectral-induced polarization (SIP) allows to measure polarization of materials in addition to electrical conduction. The estimated property is the complex electrical resistivity in which both magnitude (resistivity) and phase shift are measured for a range of frequencies. The imaging extension of SIP is referred to as electrical impedance tomography (EIT). Electrical impedance here refers to the effective resistance to an alternating current due to the combined effect of ohmic resistance and reactance. SIP and EIT have been successfully used in biogeophysical investigations involving microbial processes (Abdel Aal et al., 2004, 2006; Atekwana & Slater, 2009; Atekwana et al., 2006; Kessouri et al., 2019), structural characterization of wood (Martin, 2012; Martin et al., 2015), mapping of tree roots (Mary et al., 2016), and characterization of crop roots (Ehosioke et al., 2020; Kessouri et al., 2019; Tsukanov & Schwartz, 2020; Weigand & Kemna, 2017, 2019). Despite the significant improvements presented in these recent studies, there is still a knowledge gap regarding the electrical response of fine roots at the segment scale. Improved understanding of root electrical properties is essential to help account for the effect of roots in the estimation of soil moisture content of vegetated soil and to improve noninvasive characterization of root systems. However, available experimental setups need to be adapted to allow the determination of the complex electrical resistivity of roots and root segments without incorporating the response from the plant stem.

The objective of this paper is to investigate how the complex electrical properties of root segments change with age, type of root (primary roots), and plant species. For this, a novel SIP sample holder was developed and validated. Subsequently, SIP measurements were made on Brachypodium (*Brachypodium distachyon* L.) and Maize (*Zea mays* L.) root segments of different ages.

2. Electrical Polarization of Plant Roots

It has been postulated that polarization occurs both at the outer root surface (root-soil interface) and in the inner root system (Weigand & Kemna, 2019). In general, polarization is due to the presence of the cell membranes that act as capacitors. Polarization at the outer root surface depends on the concentration of ions in the external fluid while that of the inner root system depends on the ionic composition of the cellular fluid (Weigand & Kemna, 2017, 2019). This implies that the complex resistivity magnitude and phase spectra could be useful for noninvasive characterization of roots. Mary et al. (2017) and Weigand and Kemna (2017) have shown that SIP measurements are promising for root system characterization as they both reported a low-frequency (<1 kHz) polarization of a coarse root in the laboratory and a crop root system in a rhizotron, respectively. Tsukanov and Schwartz (2020) found a linear correlation between root biomass and electrical polarization at low frequencies (<1 kHz), and also demonstrated the relationship between root polarization and root cell membrane potential. Most studies have focused on low-frequency polarization and therefore the mechanisms responsible for polarization at high frequencies (>1 kHz) in roots are yet to be understood.

Ehosioke et al. (2018) and Kessouri et al. (2019) reported strong polarization at high frequencies (≈10 kHz) for Maize (*Z. mays* L.) roots, suggesting that polarization in roots is not limited to low frequencies. Some studies (e.g., Bera et al., 2016; Repo et al., 2012) have shown that current pathways in roots are different at low and high frequencies because the cell membrane does not allow current passage at low frequencies (Figure 1b). As cell
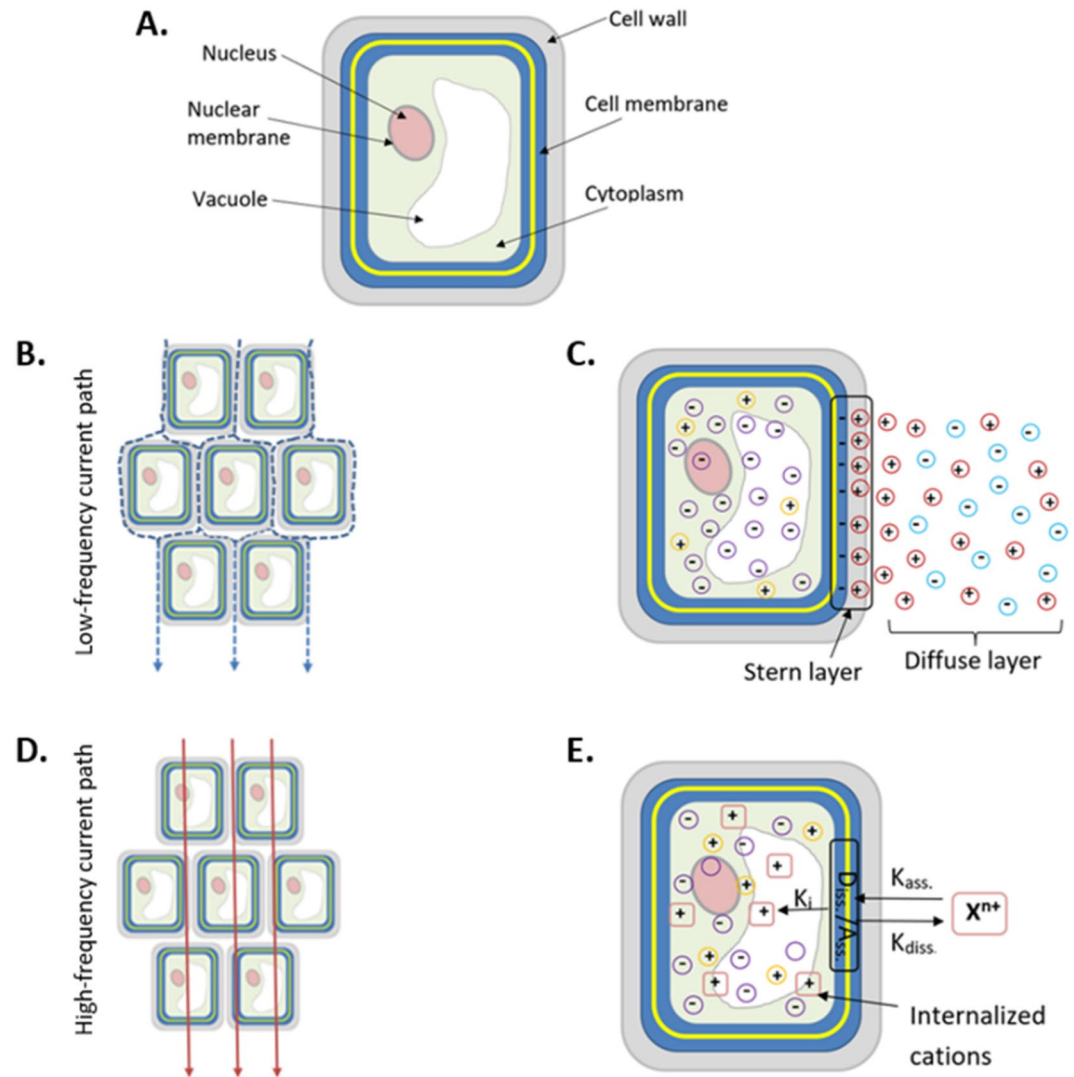
Figure 1. Cell-based conceptual model describing polarization mechanisms in root segments. (a) Schematic illustration of a plant cell showing the extracellular and intracellular components. (b) Low-frequency current path (apoplastic pathway) in the root through the apoplastic space filled with extracellular fluid (ECF), without crossing the cell membrane. (c) Illustration of counter-ion polarization mechanism in root segments occurring at low frequencies (e.g., Weigand & Kemna, 2019). Counter-ion polarization is based on the strength of the electrical double layer (EDL), which depends on the ionic composition of the ECF and the electric potential distribution at the cell membrane. (d) High-frequency current path (symplastic pathway) in the root with current crossing both extracellular and intracellular cell components and the cell membranes. (e) Illustration of interfacial polarization mechanism in root segments occurring at high frequencies based on Wang et al. (2011). This involves a process of dissociation/association occurring at the cell membrane, which depends on the ionic concentration gradient between the ECF and ICF (X^{n+} is a conceptualized cation, K_{diss}, K_{ass}, and K_{int} are the dissociation, association, and internalization rate constants).

membranes become more conductive at higher frequencies, current passes through the entire cell (Figure 1d). Therefore, the impedance response is determined by the ratio of the two current pathways within the root and the frequency of the alternating current. This explains the different polarization behavior at low and high frequencies reported in different studies (e.g., Ehosioke et al., 2018; Kessouri et al., 2019), which corresponds to counter-ion and interfacial polarization mechanisms in biomaterials as described by Schwan and Takashima (1991) and Kao (2004). Counter-ion polarization due to ionic diffusion in the electrical double layer (EDL) adjacent to charged surfaces typically occurs below 20 kHz (Kao, 2004; Schwan & Takashima, 1991). Interfacial polarization occurs due to restricted movement of ions in the intercellular space as a result of complex structural properties of biological tissue, which creates high conductivity zones within a matrix of low conductivity material (e.g.,

cell interiors surrounded by cell membranes). Interfacial polarization typically occurs in the kHz-MHz frequency range (Kao, 2004; Schwan & Takashima, 1991).

Conceptual models have been proposed to describe polarization in roots (e.g., Kessouri et al., 2019; Weigand & Kemna, 2019) based on the work of Wang et al. (2011), which outlined the dual effect of cell membrane surface potential including the EDL formation and transport across the cell membrane through an active binding site where dissociation/association occurs. The active binding site (i.e., voltage gated ion channels) of the cell membranes are closed at low frequencies because a low-frequency electric field produces changes in the membrane potential difference that are too small to significantly alter the properties of the ion channels (Mathie et al., 2003). The EDL prevents passage of current through the cell membrane (i.e., the impedance of the cell membranes is so high that it does not allow current passage). In this case, the current passes through the apoplastic pathway (Bera et al., 2016; Ehosioke et al., 2020; Repo et al., 2012), as shown in Figure 1b. The total impedance in this low-frequency case is mainly determined by the ionic composition of the extracellular fluid (ECF) and electric potential distribution at the cell membrane (Bera et al., 2016; Repo et al., 2012); this is known as "counter-ion polarization" (Figure 1c). At high frequencies, the applied electrical field at the outer surface of the membrane changes the transmembrane potential difference that regulates the gating of ion channels and ion fluxes across the cell membranes (Hille, 2001; Kinraide, 2001; Mathie et al., 2003). The ion channels are opened which leads to decreased negativity of the membrane surface potential and an increased cation flux into the cell that results in a weaker EDL (Kessouri et al., 2019; Kinraide, 2001; Kinraide & Wang, 2010; Wang et al., 2011; Weigand & Kemna, 2019), and a lower polarizability of the EDL. At these high frequencies, current flows through the symplastic pathway, crossing the entire cell and different interfaces (Figure 1d). In this case, the resulting total impedance will be a combination of the properties of the apoplast and the ECF, the cell membranes, the cytoplasm, and the ICF (Bera et al., 2016; Ehosioke et al., 2020; Repo et al., 2012). The polarization is therefore considered to be interfacial (Figure 1e).

3. Materials and Methods

3.1. Development and Validation of SIP Measurement Setup

SIP measurements were made using a four-electrode setup where two electrodes are used to inject sinusoidal current (I_ω) into a sample and two other electrodes are used to measure the potential difference or voltage (V_ω). This provides a complex frequency-dependent electrical impedance (Z_ω^*) expressed as

$$Z_\omega^* = \frac{V_\omega}{I_\omega} = Z_\omega' + j Z_\omega'' \tag{1}$$

where ω is the angular frequency, Z' and Z'' are the real and imaginary parts of the complex impedance, and j is the imaginary number. The complex resistivity (ρ^*) is an effective material property obtained from the measured complex impedance using a geometric factor K determined by the positions of the current and potential electrodes

$$\rho_\omega^* = K Z_\omega^* = \rho_\omega' + j \rho_\omega'' = |\rho| (\cos \varphi + j \sin \varphi) = |\rho| e^{j\varphi} \tag{2}$$

where ρ' and ρ'' are the real and imaginary parts of the complex resistivity, $|\rho|$ is the resistivity magnitude, and φ is the phase shift.

The SIP measurement system used in this study consists of a function generator, an amplifier unit, a data acquisition (DAQ) card, a computer, and a sample holder (Figure 2). The function generator (model 33511B, Keysight technologies) was used to generate a sine wave stimulus voltage with adjustable amplitude and frequency. The voltages at the electrodes were measured with short triaxial cables (0.5 m) and a high-impedance DC coupled amplifier (ZEA-2-SIP04-V05) as described by Zimmermann et al. (2008). The triaxial cables were used with a driven shield (Morrison, 1998) to reduce parasitic current leakage and capacitive loads. The amplifier unit contains a shunt resistor R_s (1 kΩ) for the current measurement. The voltages were digitized using a 4-channel USB based DAQ card (NI USB-4431). This is a 24-bit Sigma-Delta-DAQ card with digital antialiasing filters and high phase accuracy. The oversampling rate is 64 at a maximum sampling rate of 102 kHz. The measurements were performed in the frequency range between 1 Hz and 45 kHz using a voltage of 5 V. The resolution of 24-bit (1.2 µV) allows for the measurement of AC voltages with an acceptable signal-to-noise ratio. The cross talk of the DAQ card is smaller than −90 dB (shorted input). DAQ and postprocessing were performed with custom-made
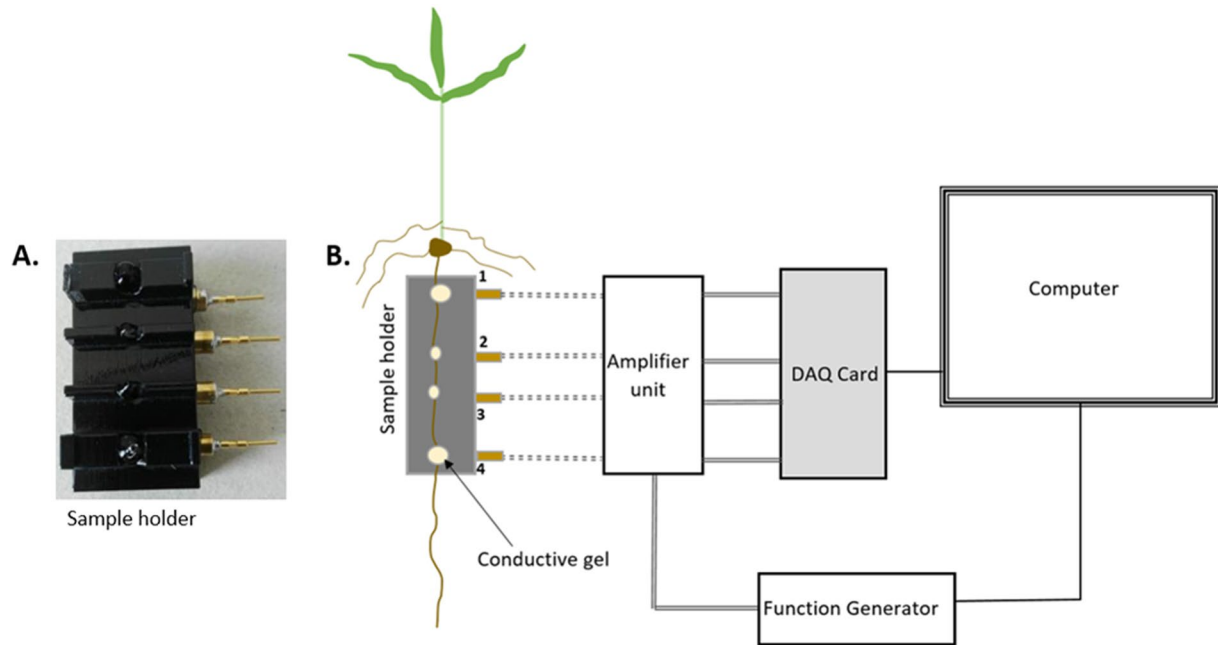
Figure 2. The measurement setup. (a) The new sample holder for spectral-induced polarization (SIP) measurements on root segments showing the retracted brass electrodes and the channels filled with conductive gel. (b) Schematic illustration of the SIP measurement setup consisting of a sample holder, amplifier unit, function generator, data card, and a computer.

LabVIEW and MATLAB programs, respectively. The LabVIEW program controls the function generator and the DAQ card and stores each measurement frequency and time series of the voltages $u(t)$.

A root sample holder was designed to determine the complex impedance of root segments of 4-cm length with a diameter up to 2 mm. The sample holder is a 3D printed rectangular plastic block with four-electrode channels (1.5 cm apart) on one side that allows for seamless insertion of four cylindrical brass electrodes, and the positioning of a single root segment on top of the sample holder perpendicular to the electrode channels (Figure 2a). The electrode channels are filled with a conductive gel (Rodisonic contact gel, Pannoc Nv, Belgium) to ensure a good electrical contact between the root and the electrode. The gel is injected from the side of the sample holder and is pushed into the channel by the electrodes to exclude air bubbles. The root is mounted on the sample holder in such a way that the contact with the electrodes is established through the conductive gel. The potential electrodes were kept outside the current path to avoid the influence of electrode polarization. In addition, this design avoids injuring plants by pushing electrodes into the tissue, which possibly generates induced electrical signals (Julien et al., 1991; Meyer & Weisenseel, 1997; Roblin, 1985).

Correction of the measured voltages is required to minimize the error due to high contact resistances. The true sample impedance is given by

$$Z_x = \frac{U_x}{I_x}. \tag{3}$$

It can only be calculated if the true voltage U_x and true current I_x are known. It is therefore necessary to resolve the discrepancies between the true and measured current (I_x and I_m) and the true and measured voltage (U_x and U_m) using an electrical circuit model of the sample and the measurement system (Figure 3). By measuring the current with a shunt resistor between electrode 4 and the ground, the true current I_x can be calculated using the known impedances Z_v and the ground-based measured voltages U_3 and U_4 (Zimmermann et al., 2008)

$$I_x = I_s + I_3 + I_4 = \frac{U_4}{R_s} + \frac{U_3}{Z_v} + \frac{U_4}{Z_v} \tag{4}$$

The discrepancy between the measured voltage $U_m = U_2 - U_3$ and the true voltage U_x results from the load of the amplifier Z_v and the impedances Z_{e2} and Z_{e3}. The leakage currents I_2 and I_3 cause a voltage drop at the contact
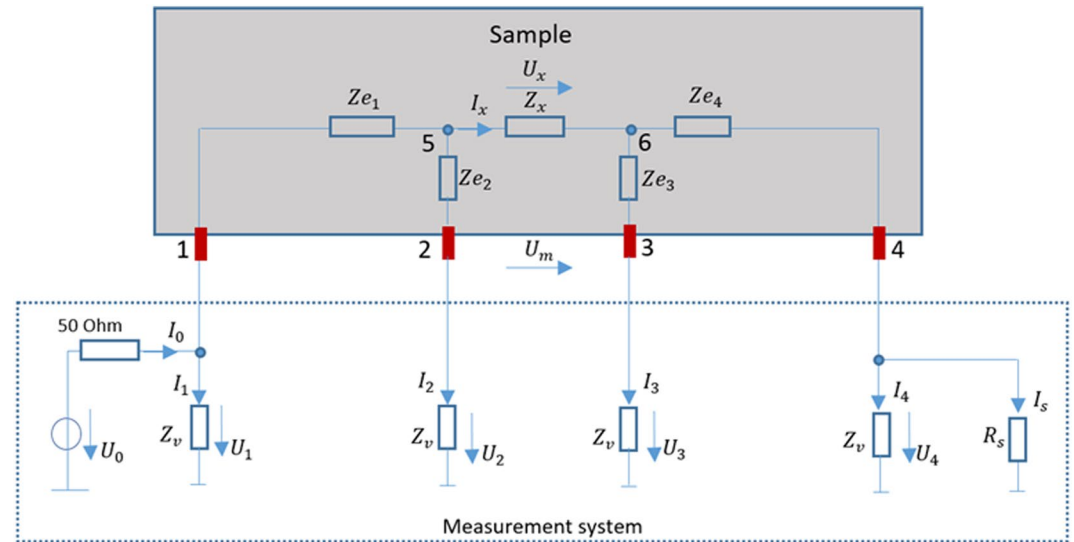
Figure 3. Electrical model of the measurement setup. Z_x, U_x, and I_x are the true sample impedance, true voltage, and true current, respectively. Z_{e1} and Z_{e4} are the contact impedances at the current electrodes and sample interface, while Z_{e2} and Z_{e3} are the contact impedances at the potential electrodes. U_0 and I_0 are the source voltage and input current, respectively. I_s is the current at the shunt resistor, Z_v is the input impedance of the amplifier and the cables, R_s is the shunt resistor, and U_m is the measured voltage. U_i denotes the ground-based measured voltages, while I_i denotes the parasitic leakage currents (modified from Zimmermann et al. (2008)).

impedances Z_{e2} and Z_{e3}, which is responsible for the voltage difference between U_x and U_m. By estimating the impedances Z_{e2} and Z_{e3} during measurements, the true voltage $U_x = U_5 - U_6$ can be calculated as described by Zimmermann et al. (2008) and Huisman et al. (2016)

$$U_x = U_2 \left(1 + \frac{Z_{e2}}{Z_v}\right) - U_3 \left(1 + \frac{Z_{e3}}{Z_v}\right) \tag{5}$$

The contact impedances Z_{e2} and Z_{e3} usually depend on the measurement object and are therefore unknown. They can be determined in situ using the method described in Huisman et al. (2016) where a reciprocal measurement is made with a current injection at electrodes 2 and 3 and a voltage measurement at electrodes 1 and 4. With this additional measurement to determine Z_{e2} and Z_{e3}, the true voltage U_x on the sample can now be calculated using Equation 5.

The performance of the measurement setup was evaluated using four ideal resistors (10, 100, 900 kΩ, and 4.7 MΩ). The resistors were selected based on the range of resistances previously reported for root segments (e.g., Anderson & Higinbotham, 1976; Cao et al., 2010; Ehosioke et al., 2017). The measured impedance values for the resistors matched the known impedance values (Figure 4a). In addition, the 10, 100, and 900 kΩ resistors showed no phase response for frequencies below 1 kHz (Figure 4b) as expected for an ideal resistor, with an error of 0.001 rad at 10 kHz. The 4.7 MΩ resistor showed phase errors up to 0.005 rad between 1 and 10 kHz, but this is small compared to the expected signals from the root segments. The experimental setup and the newly designed sample holder are therefore suitable for characterizing the electrical properties of root segments.

3.2. Plant Growth and Measurement Procedures

To determine the electrical properties of root segments, 30 Brachypodium (*B. distachyon* L.) and 30 Maize (*Z. mays* L.) plants were grown in plastic tubes of 5-cm diameter and 20-cm height filled with a mixture of fine and coarse sand with a grain size distribution ranging from 0.1 to 1.0 mm to allow easy cleaning of the roots prior to the SIP measurements. The plants were watered with tap water at 2-day intervals and they all had three leaves at the end of the experiment except one Maize plant that had four leaves. SIP measurements were made on the primary roots (see Appendix A) on 10 sampling days between 8 and 29 days after sowing (DAS). At each sampling day, three replicates were analyzed (A, B, and C), which resulted in the total number of 30 plants for each species. Before making SIP measurements, the root was first cleaned with deionized water and dried with tissue paper. Next, the root was mounted in the sample holder and the diameter was measured with a digital caliper. SIP measurements were made using normal and reciprocal electrode configurations as described above. It
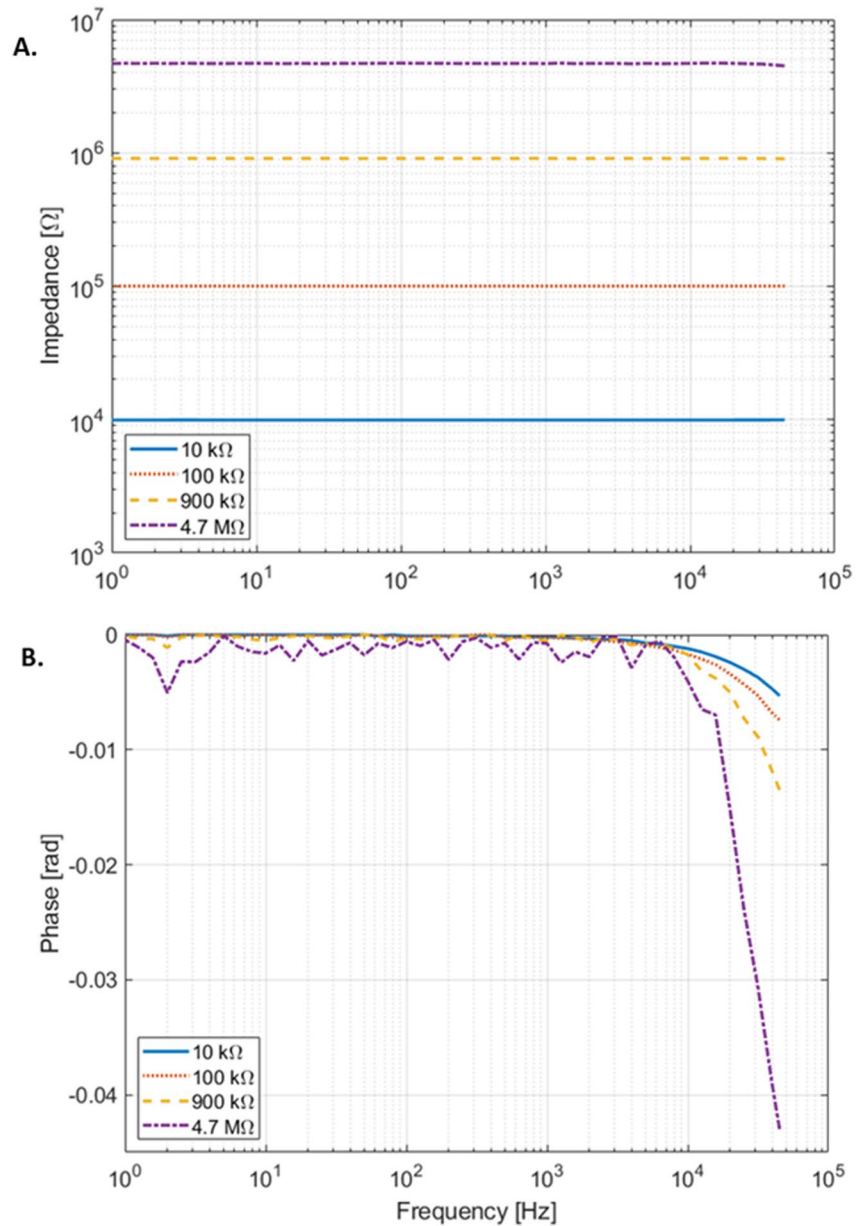
Figure 4. Validation of measurement setup. (a) The measured impedance magnitude and (b) the measured phase response for the ideal resistors.

was ensured that electrode 1 was always close to the root collar. The axial electrical resistivity of the root segment ρ_r (Ωm) was calculated from the measured electrical impedance using

$$\rho_r = Z_r \frac{\pi D_r^2}{4L_r} \tag{6}$$

where Z_r is the electrical impedance of the root segment, D_r is the diameter of the root segment, and L_r is the length of the root segment between the potential electrodes (1.5 cm).

3.3. Microscopic Sections of Root Samples

After each SIP measurement on a root segment, a root sample was excised at the exact measurement location (at the collar) and preserved in a fixing solution for later microscopic analysis. Maize root samples were fixed
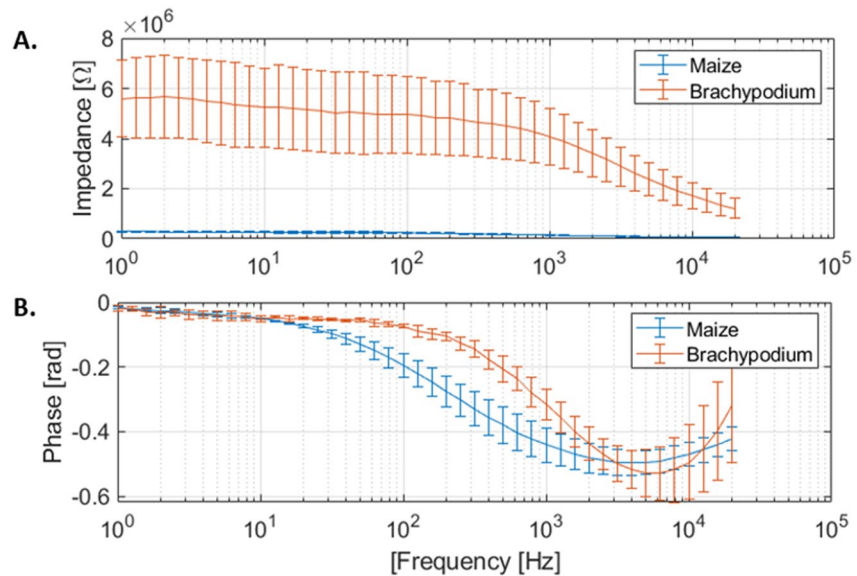
Figure 5. Average electrical responses of several Maize and Brachypodium roots at 8 DAS (a) average impedance magnitude and (b) average phase.

in methanol before being embedded in paraffin. Due to the small size and fragility of Brachypodium roots, they were fixed in 4% paraformaldehyde (PFA) and then embedded in paraffin-agar. Thin sections of 5 μm were obtained from the root samples using a microtome (Microm HM355S, ThermoFisher, Geel, Belgium). The thin sections were mounted on a glass slide and stained with hematoxylin and eosin (H&E) for easier identification of the cellular features. The stained sections were scanned using a microscope at 40× magnification (Nanozoomer S360, Hamamatsu, Herrsching am Ammersee, Germany). The scanned images were analyzed using RootAnalyzer (Chopin et al., 2015) to obtain characteristic cellular features.

4. Results and Discussion

4.1. Impedance and Phase Response of Root Segments

The average complex impedance of the Maize and Brachypodium roots at 8 DAS is shown in Figure 5. The impedance magnitude of Maize roots is relatively low (284 kΩ) compared to that of Brachypodium (5,600 kΩ). Therefore, larger phase errors are expected for the Brachypodium roots. The average maximum phase response of the root segments at 8 DAS is 0.49 rad at 3.9 kHz and 0.53 rad at 6.3 kHz for Maize and Brachypodium, respectively, which implies that the signal is higher than the measurement errors (Figure 4). This indicates that the observed polarization is mainly from the roots and not due to electromagnetic coupling effects. The polarization peaks occur at ~10 kHz, which is very high compared to the low-frequency polarization peaks reported by several other studies for larger diameter roots (Table 1).

Table 1
Electrical Resistivity and Polarization Response of Various Species

| Reference	Species (diameter)	Water content (%)	Resistivity (Ωm)	Phase peak (mrad)	Frequency of the peak (Hz)
Schleifer et al. (2002)	Ash (20 mm)	Saturated	70	70	6
Zanetti et al. (2011)	Poplar (6–7 cm)	≈50	50	20	0.1
Martin (2012)	Oak (20 mm)	≈20	166	33	0.01
Mary et al. (2017)	Poplar (35 mm)	17	731	9	0.2
This study	Maize (8 DAS) (0.82 mm)	Saturated	16.5	490	3,900
	Brachypodium (8 DAS) (0.24 mm)	Saturated	33	670	7,900
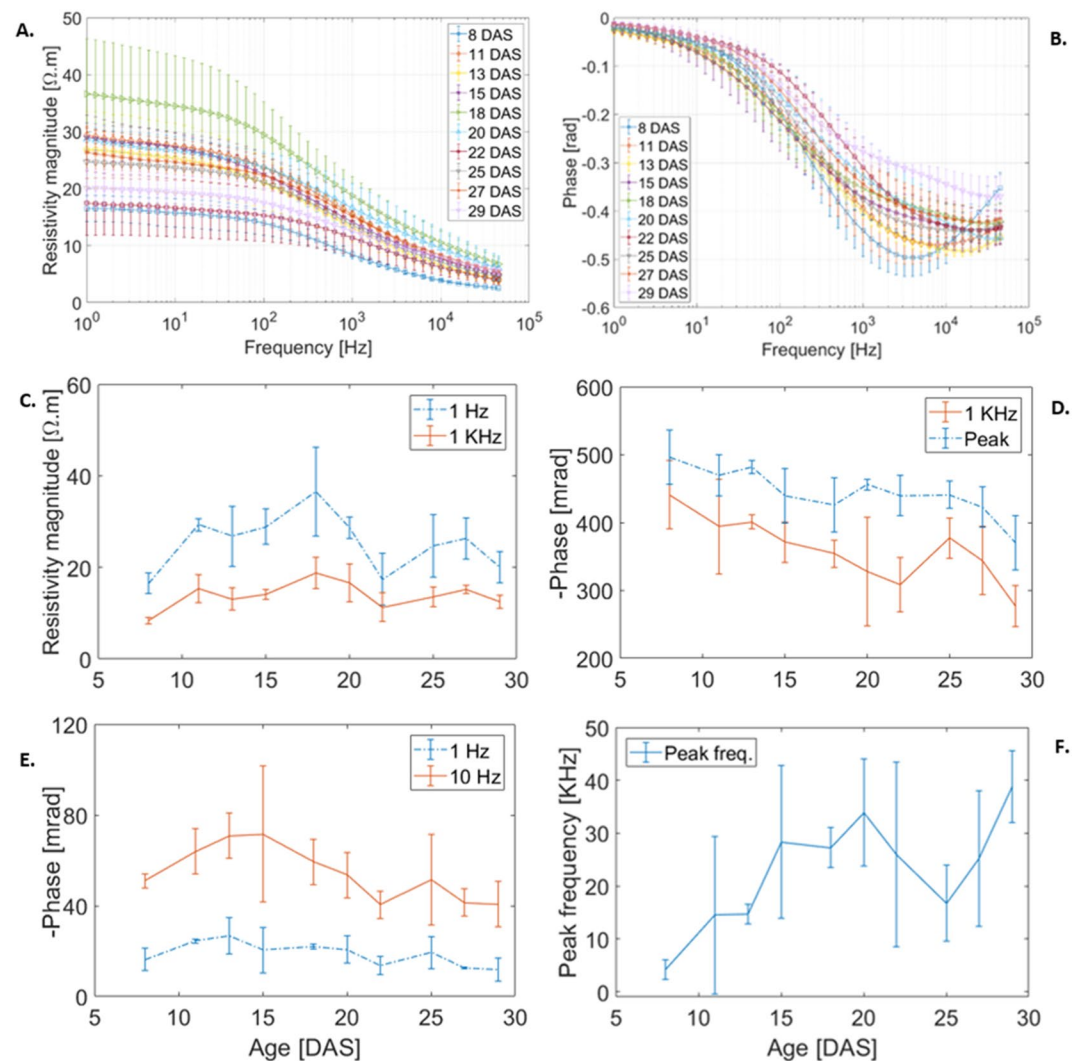
Figure 6. Age effect on spectral-induced polarization of Maize primary roots. (a and b) The average resistivity magnitude and phase response at 10 different ages, with error bars indicating the standard deviation of the replicates. (c) Average resistivity magnitude at 1 Hz and 1 kHz. (d) Average phase response at the peak frequency and 1 kHz. (e) Average phase response at two low frequencies (1 and 10 Hz) showing a different response compared to that at high frequencies. (f) Average peak frequency.

4.2. Effect of Age on the SIP Signature of Roots

The effect of age on the electrical properties of Maize and Brachypodium roots is shown in Figures 6 and 7, respectively. For both root types, the resistivity magnitude varied less among replicates at higher frequencies above 1 kHz (Figures 6a and 7a), while the phase values varied less at lower frequencies below 1 kHz (Figures 6b and 7b). The resistivity of Maize roots did not show a clear trend with age. At 1 Hz, it seemed to increase up to 18 DAS, after which the resistivity magnitude varied considerably. At 1 kHz, no clear trend was visible (Figure 6c). A one-way ANOVA test revealed statistically significant differences in mean resistivity magnitude between ages at 1 Hz and 1 kHz (both $p = 0.007$). A post-hoc analysis of the ANOVA results showed a statistically significant increase in resistivity only between 8 and 18 DAS at 1 Hz ($p = 0.018$) and 1 kHz ($p = 0.004$). The phase showed a statistically significant decrease with root age at the peak frequency ($p < 0.001$) and at 1 kHz ($p = 0.035$) (Figure 6d). At low frequencies (1 and 10 Hz), no trend in the phase response of Maize roots was observed, and no statistically significant difference was found (Figure 8e). The peak frequencies (Figure 6f) showed a statistically significant increase ($p = 0.039$), between 8 and 29 DAS. Cseresnyes et al. (2018) also observed an age-dependent decrease in phase response of intact Maize root systems, which was attributed to stress. The decrease in phase
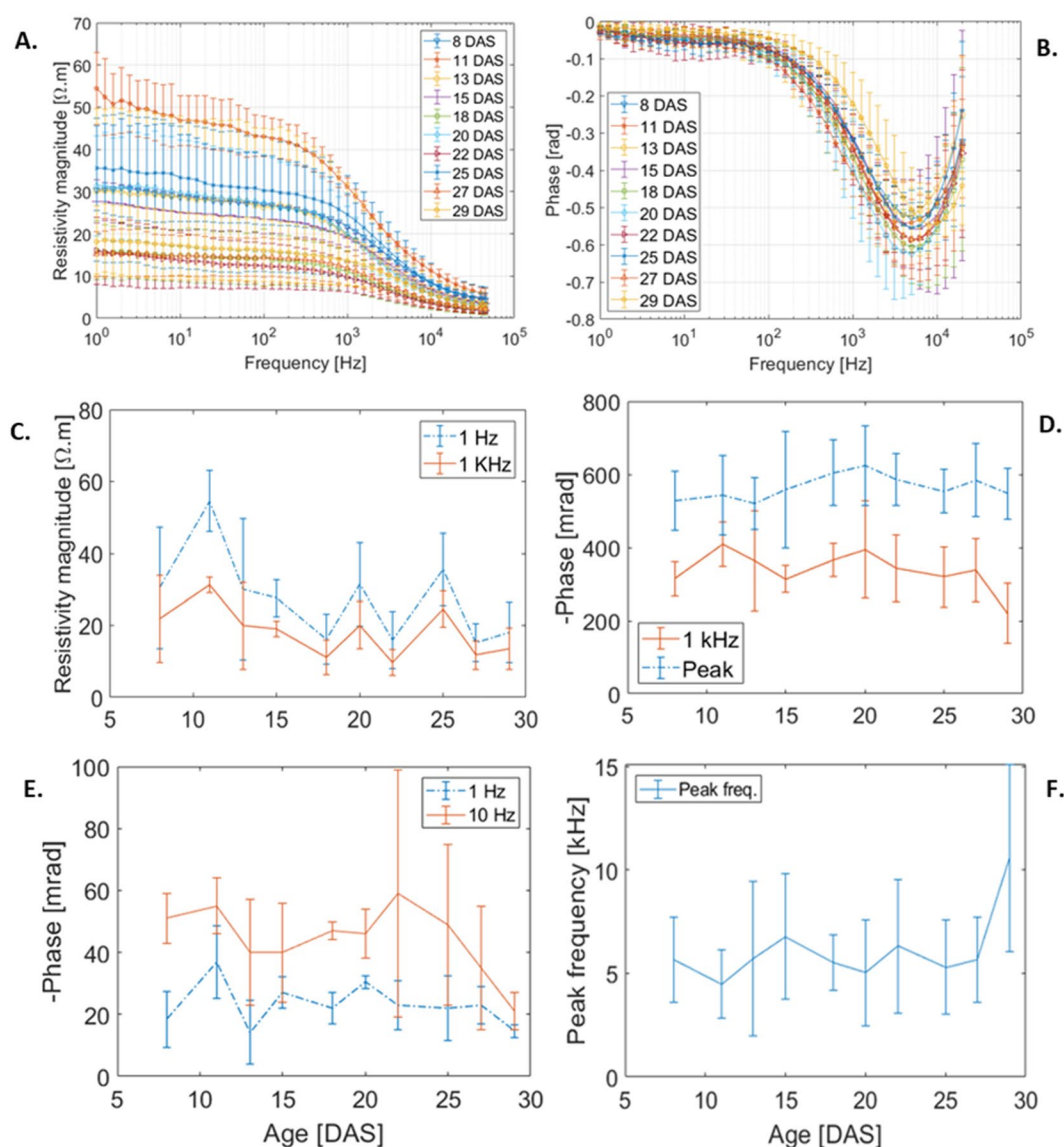
Figure 7. Age effect on spectral-induced polarization of Brachypodium primary roots. (a and b) The average resistivity magnitude and phase response at 10 different ages, with error bars indicating the standard deviation of the replicates. (c) Average resistivity magnitude at 1 Hz and 1 kHz. (d) Average phase response at the peak frequency and 1 kHz. (e) Average phase response at 1 and 10 Hz showing a different response compared to that at high frequencies. (f) Average peak frequency.

with age we observed is considered to be due to aging related stress, which is known to influence the dielectric properties of root tissues by altering the relative contribution of the apoplastic and symplastic pathways to the impedance magnitude and phase shift (e.g., Aubrecht et al., 2006; Cseresnyes et al., 2013; Li et al., 2017). Brachypodium roots showed no clear trend in resistivity magnitude, but there was an increase of the resistivity magnitude between 8 and 11 DAS at 1 Hz and 1 kHz (Figure 7c). The phase response did not change with time (Figures 7d and 7e).

4.3. Microscopic Analysis of Root Sections

Major structural changes are visible in the cortex during early stages of growth. Figure 8 shows microscopic sections of three replicate Maize roots (plants A, B, and C) at 8 and 11 DAS. The formation of Aerenchyma within the cortex of the Maize roots is clearly visible at 11 DAS. Aerenchyma are voids formed in the roots due to nonpathogenic death of cortex cells (Deacon & Henry, 1978; Schneider & Lynch, 2018). Table 2 shows the
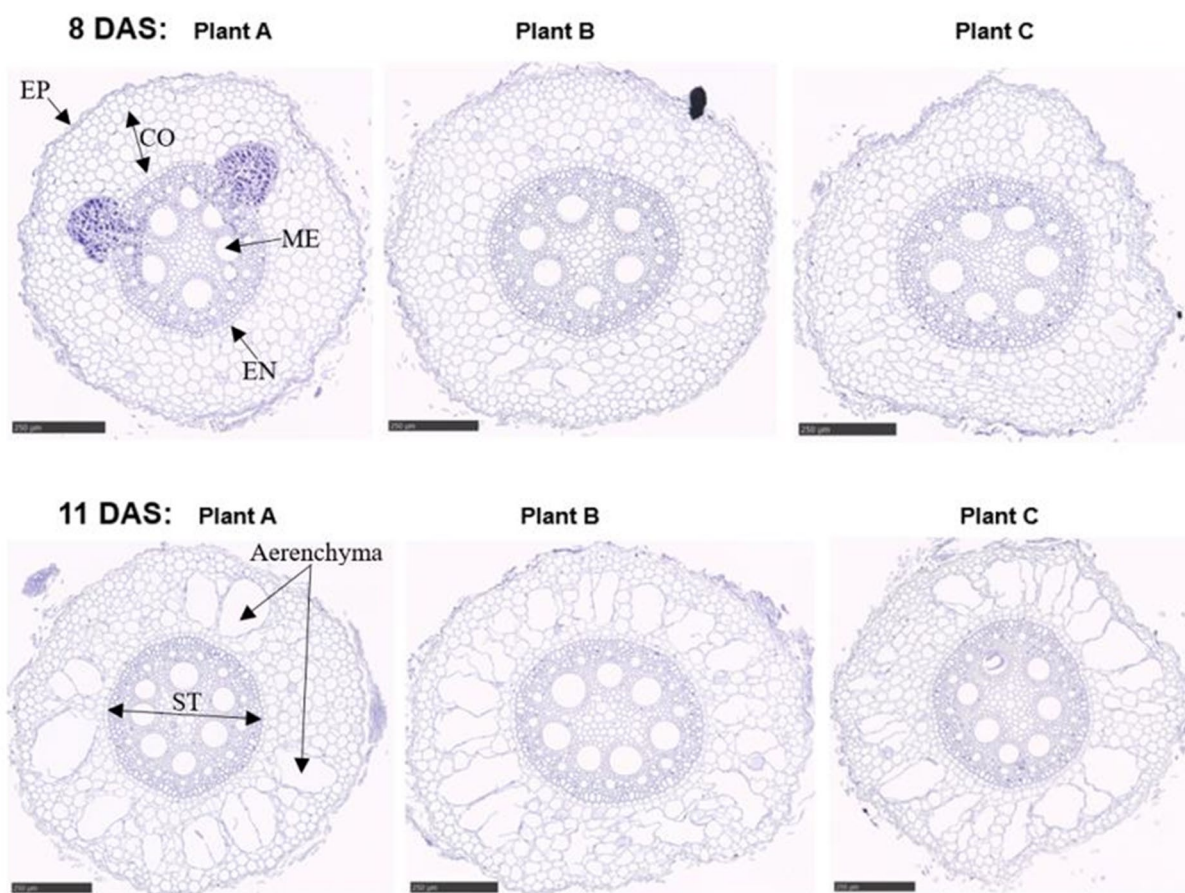
Figure 8. Microscopic sections of three replicates of Maize primary roots at 8 DAS (top) and 11 DAS (bottom) taken at 1.5-cm distance to the seed. EP is the epidermis, CO is the cortex, ME is the metaxylem, EN is the endodermis, and ST is the stele. Formation of Aerenchyma as a result of dead cortex cells is clearly visible at 11 DAS, which reduced the number and size of the cortex cells. Scale bar = 250 μm.

average size and number of various cell types of the Maize root replicates for both days. The average total root area was higher at 11 DAS than at 8 DAS. However, the average cortex area decreased. Also, the average number of cortex cells decreased by 20.6% from 8 to 11 DAS. Interestingly, the average area and number of Aerenchyma increased by a factor of 16 and 11, respectively, between 8 and 11 DAS.
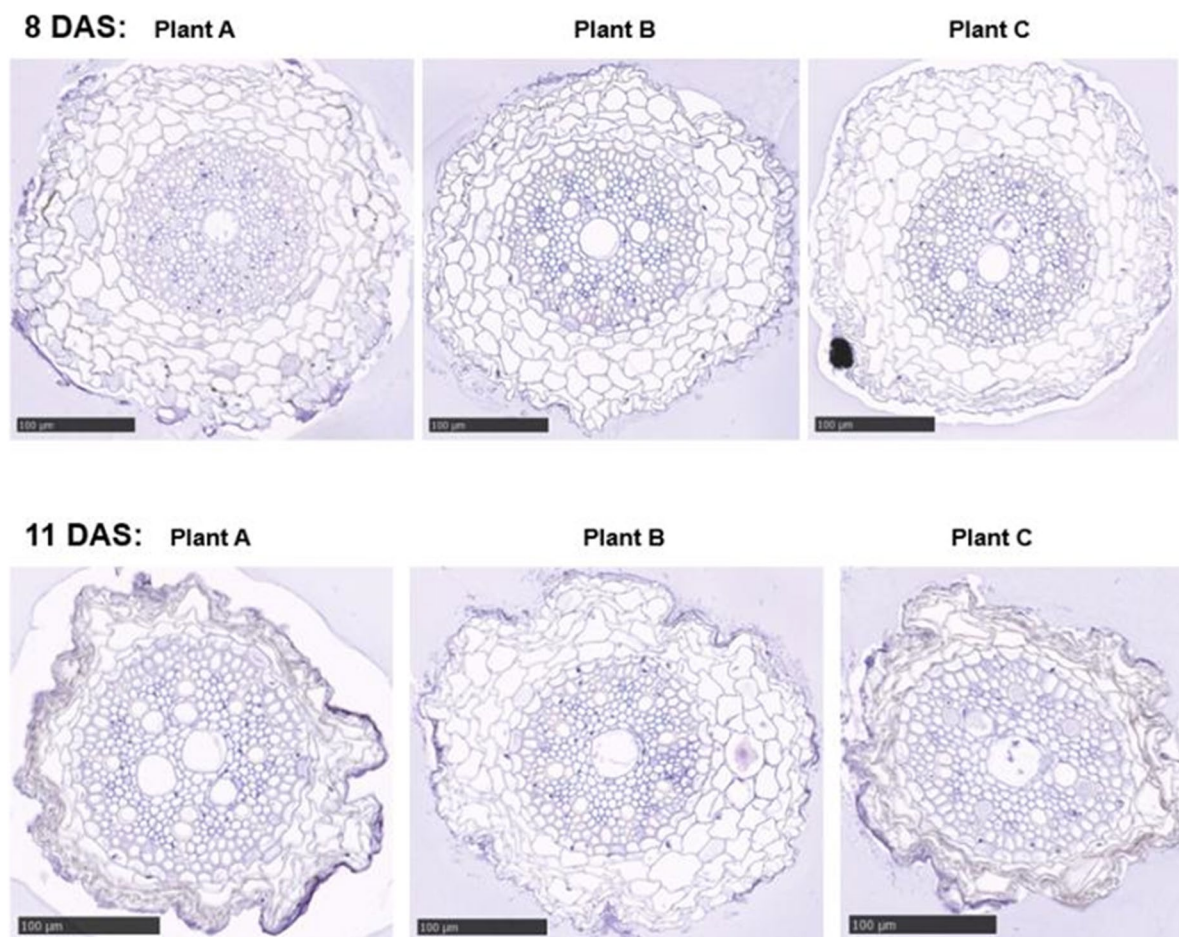
Figure 9 shows the microscopic sections of three Brachypodium roots for 8 and 11 DAS. There are no Aerenchyma in the Brachypodium roots, but rather a shrinkage of the cortex cells was observed. It is unclear if this is due to problems with the microscopic procedures or associated with structural changes in the cortex with age. Table 3 shows the average size and number of various cell types in the Brachypodium root replicates for 8 and 11 DAS. Again, the average total root area is higher at 11 DAS than at 8 DAS, while the average cortex area decreased. The average number of cortex cells in Brachypodium decreased by 29.5% between 8 and 11 DAS.

The longitudinal sections of Brachypodium and Maize roots obtained at 11 DAS are shown in Figure 10. The cortex cells of the Maize root are mostly damaged due to the formation of Aerenchyma. The longitudinal section of Brachypodium root clearly showed that the cells are continuous without damage and no Aerenchyma are present. Since our setup allows for SIP measurement on a root segment of 1.5-cm length, we do not expect major structural variations in the longitudinal section of the root that will affect our result.

Table 2
Analysis of Cross-Sections of Maize Roots at 8 and 11 DAS

| Maize	Average area (μm²)		Average number	
	8 DAS	11 DAS	8 DAS	11 DAS
Root	515,840	613,519	–	–
Epidermis	6,165	7,980	110	126
Cortex	243,742	147,693	544	432
Stele	40,947	37,673	750	805
Endodermis	5,809	5,703	76	78
Metaxylem	18,093	21,698	6	7
Aerenchyma	9,207	151,055	2	22

Figure 9. Microscopic sections of three replicates of Brachypodium primary roots at 8 DAS (top) and 11 DAS (bottom). No Aerenchyma were observed in Brachypodium. Shrinkage of the cortex was observed, but it is unclear whether it was due to mechanical damage during the microscopic procedure or if it was a structural change with age. Scale bar = 100 μm.

4.4. Linking Electrical Measurements With Microscopy Image Analysis

In a next step, the results of the electrical measurements and the microscopy image analysis are combined to obtain insights into factors affecting the electrical properties of a root segment. The percentage change in resistivity magnitude was highest (83.3%) between 8 and 11 DAS for Maize. The microscopy image analysis suggests that this is linked with the appearance of Aerenchyma in the cortex at 11 DAS (Figure 8). The direct implication of Aerenchyma formation is the reduction of the total area of living cells, while increasing the wall and void area (the difference between root area and area of cells). The wall and void density were obtained by dividing the wall and void area by the total root area, and showed a species-dependent linear correlation with resistivity magnitude at 1 Hz with Pearson correlation coefficients of $r = 0.84$ ($p = 0.018$) and 0.87 ($p = 0.011$) for Maize and Brachypodium, respectively (Figure 11). This suggests that root resistivity at 1 Hz depends on wall and void density in roots, which agrees with the results of Ellis et al. (2013) who found that the electrical impedance of a *Vicia faba* root system depends on tissue density. This is because at a low frequency of 1 Hz, current is expected to pass through intercellular spaces made up of walls and voids (Figure 1b) which are usually more resistive than the cell interior. This explains why the resistivity magnitude of roots in this study is higher at 1 Hz than at 1 kHz (Figures 6

Table 3
Analysis of Cross-Sections of Brachypodium Roots at 8 and 11 DAS

| Brachypodium	Average area (μm^2)		Average number	
	8 DAS	11 DAS	8 DAS	11 DAS
Root	319,744	444,826	–	–
Epidermis	17,597	5,246	73	54
Cortex	140,809	118,398	169	119
Stele	33,616	64,489	348	314
Endodermis	6,854	10,993	56	55
Metaxylem	2,685	5,679	1	3
Aerenchyma	0	0	0	0
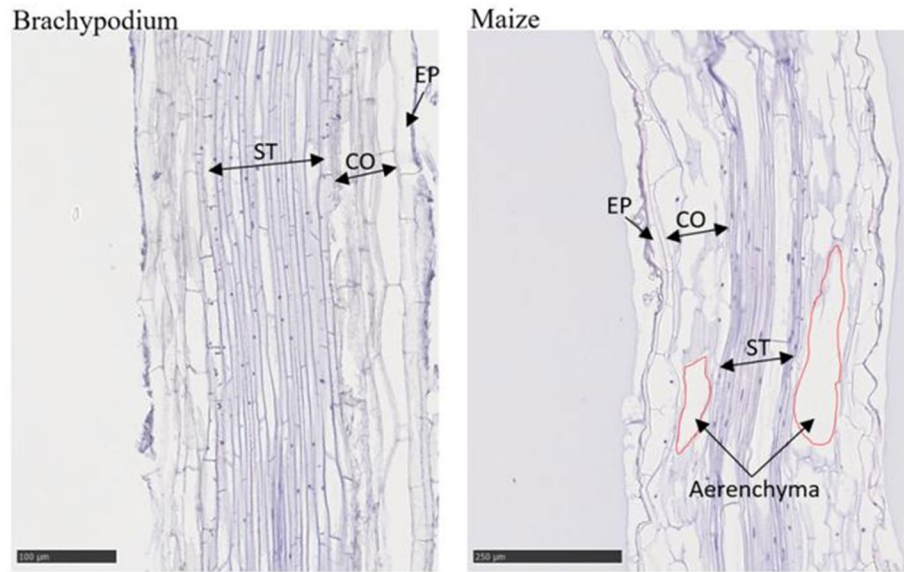
Figure 10. Longitudinal sections of Brachypodium (left) and Maize (right) primary roots at 11 DAS taken at 1.5-cm distance to the seed. EP is the epidermis, CO is the cortex, and ST is the stele. Aerenchyma are visible in the Maize cortex but absent in Brachypodium. Scale bar is 100 and 250 μm for Brachypodium and Maize, respectively.

and 7), where the current is expected to cross the cell membranes and pass through the cell interior. The structural changes such as shrinkage in Brachypodium root or Aerenchyma formation in Maize root would have increased the wall and void density (Figure 11) which led to increased resistivity at 1 Hz. The structural changes are more pronounced in Maize roots between 8 and 11 DAS and may have caused a weaker correlation in Maize compared to Brachypodium.

The relaxation times were obtained for all replicates of Maize sampled between 8 and 29 DAS. The relaxation time is defined by

$$\tau_{max} = \frac{1}{\omega_{max}} \tag{7}$$

where ω_{max} is the angular frequency at which the maximum phase shift occurs (e.g., Bücker & Hördt, 2013). A trend analysis of the decrease in phase and relaxation time with age for Maize root showed a significant correlation
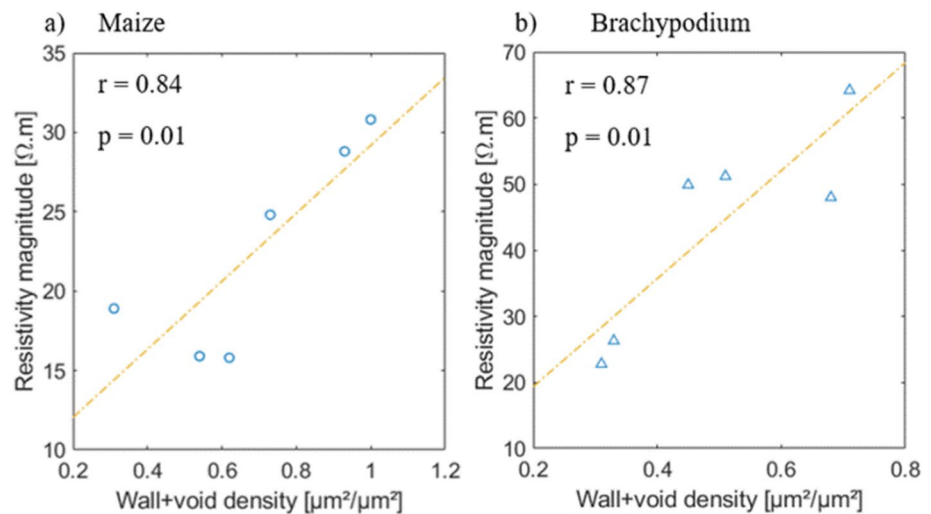
Figure 11. The relation between resistivity magnitude at 1 Hz and wall + void density in the primary roots of (a) Maize and (b) Brachypodium.
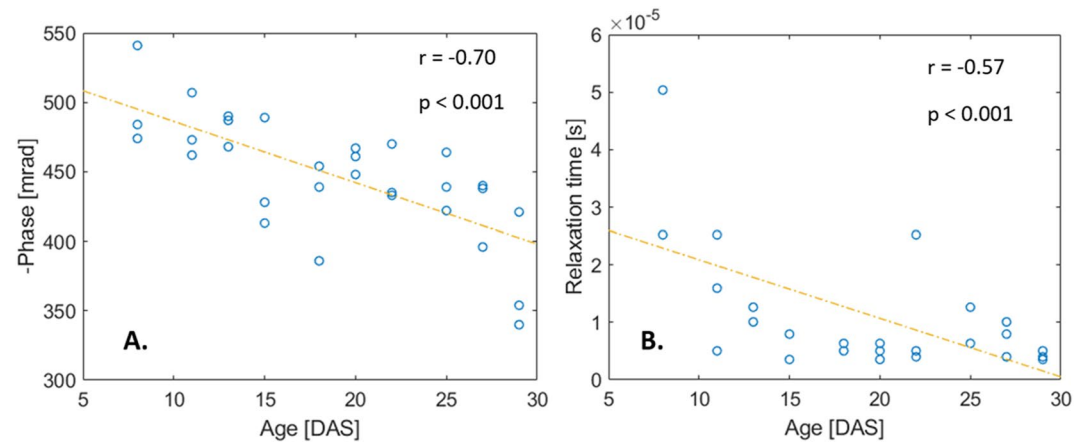
**Figure 12.** Decrease in phase peak and relaxation time with age observed in primary roots of Maize.

(Figure 12) with a Pearson correlation coefficient of $r = -0.7$ ($p < 0.001$) and $r = -0.57$ ($p < 0.001$) for phase and relaxation time, respectively. This indicates that there is an age-related decrease in polarization response of Maize roots at high frequencies above 1 kHz, which agrees with the age-related polarization changes in Maize root previously reported by Cserenyes et al. (2018). This consistent decrease in polarization with age is probably due to Aerenchyma formation because of the death of cortex cells that occurred from 11 DAS and increased until 29 DAS (see Figure B1), which would have altered the geometrical properties of the root segment as a cylindrical capacitor which was described by Dalton (1995).

At the microscopic scale, a negative linear correlation (independent of plant species) was found between phase peak and root area (Figure 13; $r = -0.70$, $p = 0.005$). When examined per species, the correlation remained significant for Brachypodium ($r = -0.72$, $p = 0.05$) but disappeared for Maize ($r = -0.45$, $p = 0.18$). Larger root area means that there are more cells in the root which should lead to stronger phase signals at high frequencies because the current passes through the entire cells, crossing various membranes (Figure 1d), thus a positive correlation is expected. The negative correlation of phase peak with root area observed here is because the root area increased by 18.9% and 39.1% between 8 and 11 DAS for Maize and Brachypodium respectively, but the area of the cortex cells decreased by 39.4% in Maize due to Aerenchyma formation that resulted from the death of cortex cells (Figure 8), and 15.9% in Brachypodium due to shrinkage (see Figure C1). These structural changes severely reduced the size of the living cells through which the current would have passed (Figure 1d) to increase the phase signal. A decrease in Phase peak with increasing wall and void density was also observed (Figures 13d–13f) for the same period which suggests that the decrease in living cells might have led to increase in wall and void density. The loss of correlation observed in Maize (Figure 13c) might be due to the larger decrease in Maize cortex area (39.4%) which is more than double that of Brachypodium (15.9%).

Relaxation time correlated positively with root area for Brachypodium roots, but showed a negative correlation for Maize roots (Figures 13h and 13i) which might be due to species effect on root electrical response. A positive correlation was found between the phase peak and cortex area in Maize (Figure 14b) between 8 and 11 DAS, but not in Brachypodium (Figure 14a). In the same period, the wall and void density correlated positively with Aerenchyma area (Figure 14e). All these are clear indications that the phase response in roots is controlled by root area with living cells.

4.5. Intraspecies and Interspecies Variability

The impedance magnitude, resistivity magnitude, and phase response of three Brachypodium and three Maize root segments at 8 DAS with an average diameter of 0.3 and 1.1 mm, respectively, are shown in Figures 15a–15f. At 1 Hz, the impedance magnitude of Brachypodium roots ranged from 4.5 to 7.4 MΩ, with an average of 5.6 MΩ and a standard deviation (SD) of 1.5 MΩ (Figure 15a), while the resistivity magnitude ranged from 18.7 to 49.9 Ωm with an average of 30.4 Ωm (SD = 12.9 Ωm) (Figure 15b). The Brachypodium roots showed strong polarization (Figure 15c) with peak values ranging from 0.45 to 0.58 rad with an average of 0.52 rad
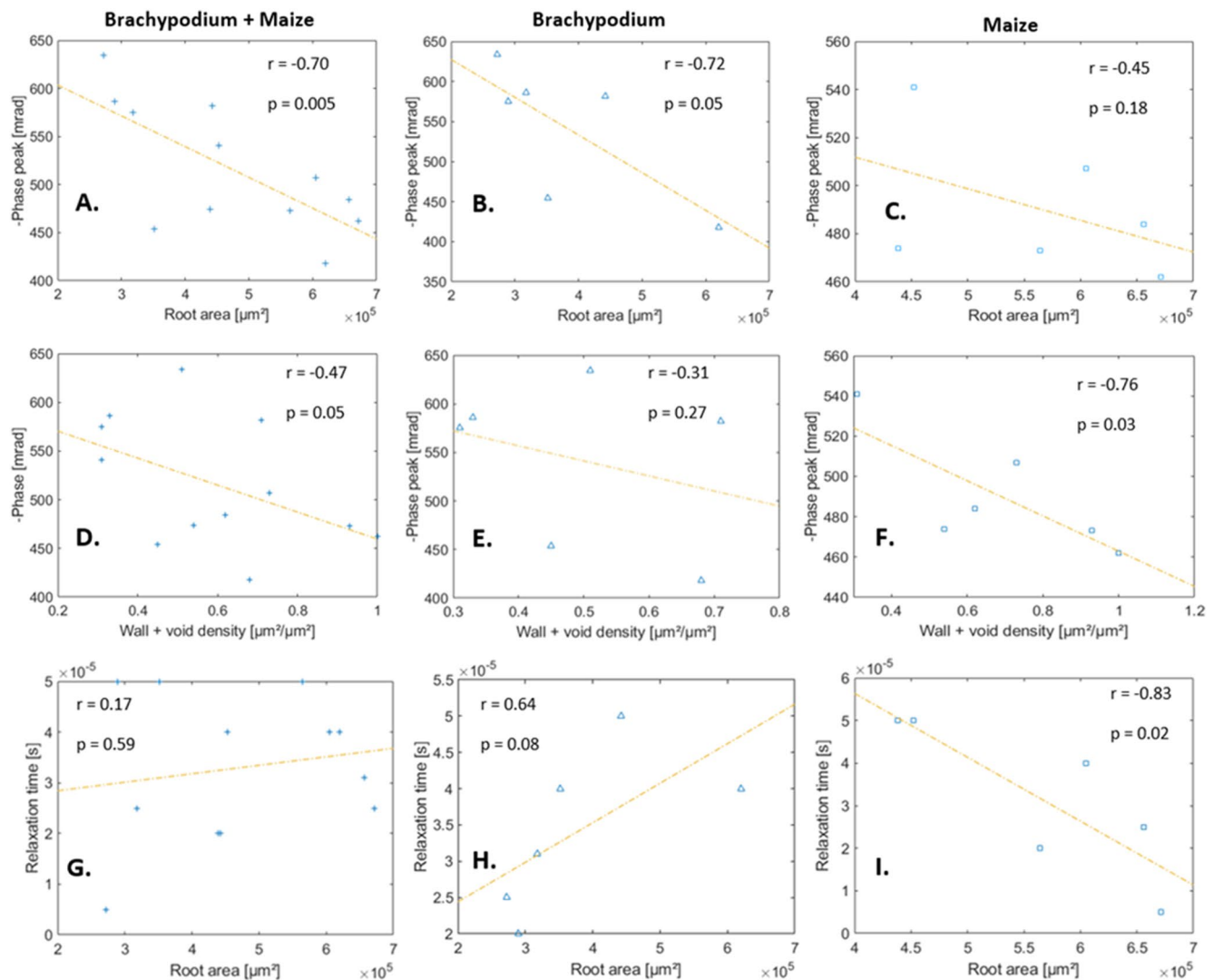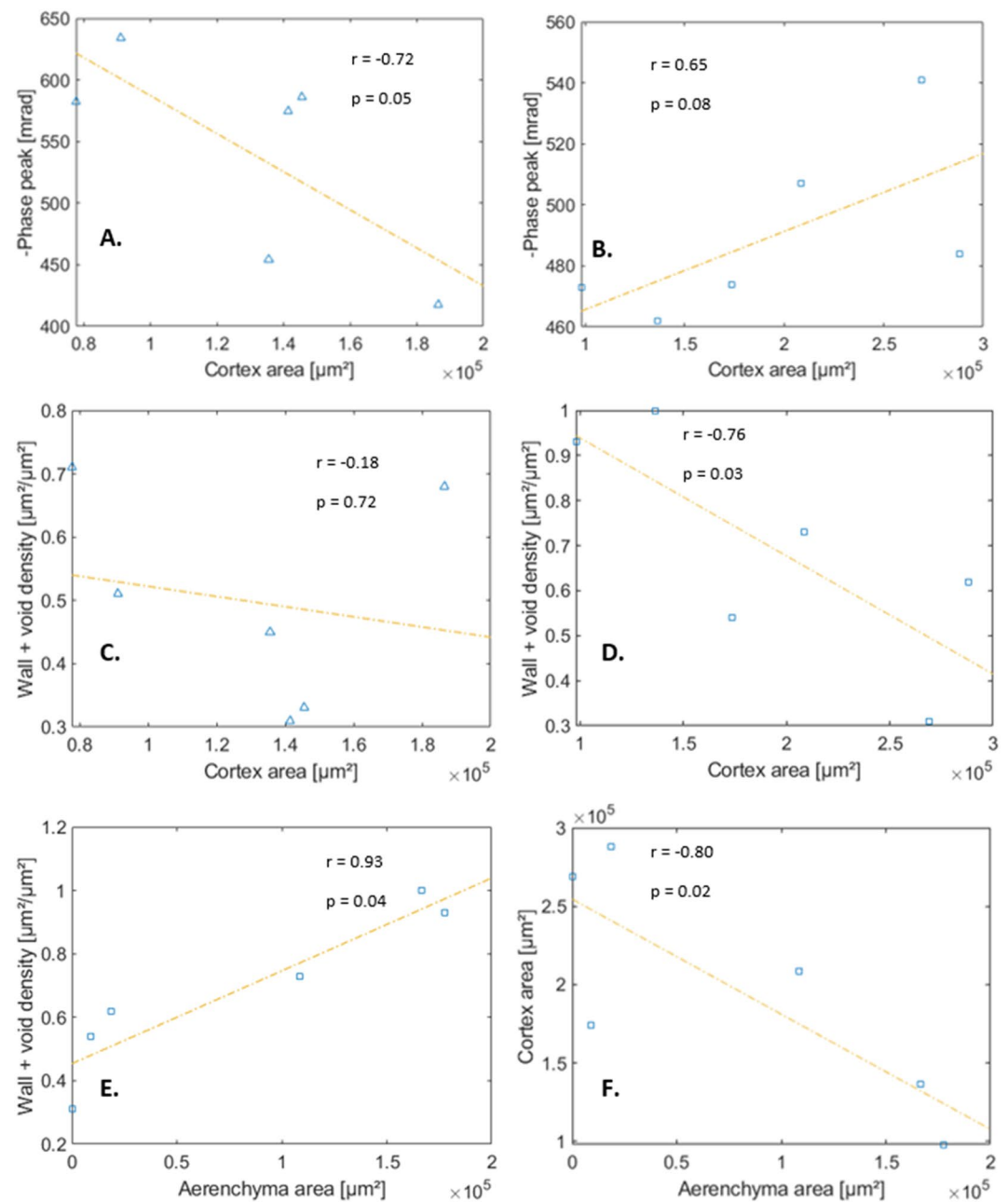
Figure 13. The relation between phase peak and total area (a–c), phase peak and wall + void density (d–f), relaxation time and root area (g–i) of primary roots of Brachypodium and Maize.

(SD = 0.08 rad) and a mean peak frequency of 6.3 kHz (SD = 1.8 kHz). The impedance magnitude of Maize roots at 1 Hz ranged from 258 to 317 kΩ with a mean value of 284 kΩ (SD = 30.4 kΩ) (Figure 15d), while the resistivity magnitude at 1 Hz ranged from 15.8 to 19.0 Ωm with a mean value of 16.5 Ωm (SD = 2.3 Ωm) (Figure 15e). Maize roots also showed a strong polarization (Figure 15f) and the peak values ranged from 0.47 to 0.54 rad with an average of 0.49 rad (SD = 0.04 rad) at a mean peak frequency of 3.9 kHz (SD = 1.8 kHz).

The results show that the impedance and resistivity magnitude of the Maize root replicates were less variable compared to Brachypodium. In addition, the average phase peak values were higher in Brachypodium (0.52 rad) than in Maize (0.49 rad) with a difference of 0.18 rad. A paired sample t-test was used to confirm that the observed difference between the phase values of both species were not significant ($p = 0.053$). However, the frequency of the phase peak was significantly higher for Brachypodium (6.3 kHz) than for Maize (3.9 kHz) ($p = 0.007$).

We expected that plants of a given species grown under identical conditions would show similar electrical signatures. It is clear from Figure 15 that different plants of the same species showed a similar shape of the SIP spectra, with higher deviations in terms of resistivity magnitude observed in Brachypodium (17 Ωm) than in Maize (2.5 Ωm). These variations in resistivity magnitude within a single species could be due to a disparity between the age of the plants which was determined as DAS and the actual age of each root replicate. Germination did not occur uniformly among all replicates so that some plants may have been younger at the time of measurement. The

Figure 14. The relation between phase peak and cortex area (a and b), wall + void density and cortex area (c and d) of Brachypodium and Maize root segments, respectively. The Aerenchyma area correlated positively with wall + void density (e) and negatively with cortex area (f) for Maize root segments.

observed intraspecies variability may also be an indication of the varying physical state of each replicate at the time of measurement. For example, one replicate could have lost more water due to evaporation before and during measurements. Future experiments should consider pregermination of seeds, selection of uniform seedlings and thinning the plants about 1 week after planting as a way to obtain a more uniform plant population that will help to minimize intraspecies variability.

Brachypodium roots had a higher resistivity magnitude and a larger phase peak at higher frequencies compared to Maize roots. This large difference between the two species is related to morphological and anatomical differences between the species as shown in Tables 2 and 3. The average area of Brachypodium primary roots was 38% smaller than that of Maize primary roots at 8 DAS and the cortex size and number were also smaller by 42%
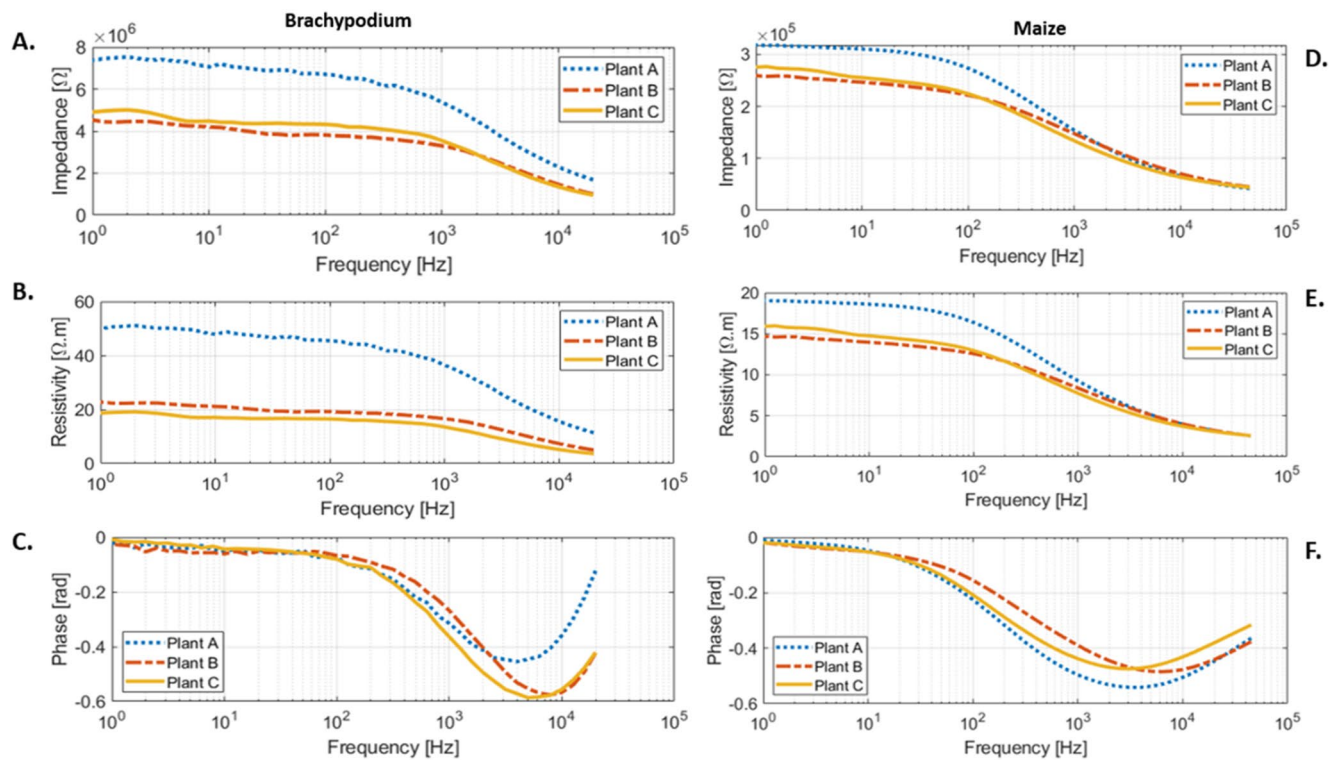
Figure 15. The impedance magnitude, resistivity magnitude, and phase responses of; (a–c) three Brachypodium roots, (d–f) three Maize roots of the same age (8 DAS) grown in the same conditions.

and 68.9%, respectively. However, the size of the epidermis in Brachypodium is 185% larger than that of Maize at 8 DAS (Tables 3 and 2). The average phase values of both species overlapped at low frequency (<10 Hz) but showed a large disparity at higher frequencies (Figures 15c and 15f).

4.6. Root Differentiation From Soils

In this study, the average resistivity of the root segments of Maize and Brachypodium at 8 DAS was 16.5 and 30.5 Ωm, respectively, while their phase values averaged 0.49 and 0.52 rad, respectively, at 10 kHz. These resistivity values are much lower than typical values for saturated sand (110–225 Ωm) and dry sand (400–1,000 Ωm) but similar to that of till (17–28 Ωm) as described by Ernston and Kirsch (2006). In field conditions, increasing temperature and fluid salinity also affects soil resistivity (Kizhlo & Kanbergs, 2009), which might make it difficult to differentiate roots from soil based on resistivity alone. The phase peak values of Maize and Brachypodium roots were found to be much higher than that of geological materials, which usually occur within the range of 0.2–20 mrad (Binley et al., 2005; Boerner et al., 1996). Even at low frequency (10 Hz), Maize and Brachypodium primary roots showed a phase response of 51 mrad (Figure 6e) and 52 mrad (Figure 7e), respectively, which is still higher than that of most geological materials. This means that fine roots of crops such as Maize and Brachypodium can potentially be differentiated from soils based on their polarization strength if sufficient root volume is present.

5. Conclusions

We presented a sample holder to determine the complex electrical resistivity of root segments in a frequency range from 1 to 45 kHz. Our results show that the electrical response of fine root segments varies with age and species. Our microscopic analysis points toward root anatomy as a controlling factor for the electrical signature of roots. The resistivity magnitude correlated with wall and void density in both species, while phase peak correlated with root area but was affected by wall and void density in Maize. A decrease in relaxation time and phase observed in Maize was linked with Aerenchyma formation which increased wall and void density while reducing

the total area of cells. This leads us to conclude that the resistive response of the root segments depends on the wall and void density while the phase response is controlled by total area of the root with living cells. It is also clear from our results that fine root segments of crops such as Maize and Brachypodium can be differentiated from soils based mainly on their stronger polarization response. Further SIP studies targeting roots at the field scale should be performed and interpretations of the results should integrate the understanding of root electrical properties at the segment scale. This will provide useful information that will help to better understand the contribution of roots to the biogeochemical dynamics of the critical zone.

Appendix A: Root Systems of Brachypodium and Maize Plants

Brachypodium (*B. distachyon* L.) and Maize (*Z. mays* L.) are both monocotyledons belonging to the Poaceae family, which is a very important family in terms of economic value. The complexity of the monocot root system depends on the species and the environmental conditions (Hardtke & Pacheco-Villalobos, 2015). However, they generally have a rather fibrous root system.

A1. Brachypodium Root System

Brachypodium has all characteristics of a monocot root system but with minimal complexity compared to other monocot species (Chochois et al., 2012; Hardtke & Pacheco-Villalobos, 2015), as shown in Figure A1a. The root system of Brachypodium consists of one axial primary root developed during embryogenesis without any seminal root, and postembryonic roots categorized as coleoptile node roots (CNR) and leaf node roots (LNR) depending on the location of emergence. The lateral LNR are sometimes absent, e.g., when Brachypodium is grown in solution (Poire et al., 2014). The primary root and CNR are always present and active for the entire life span of the plant (Hardtke & Pacheco-Villalobos, 2015).
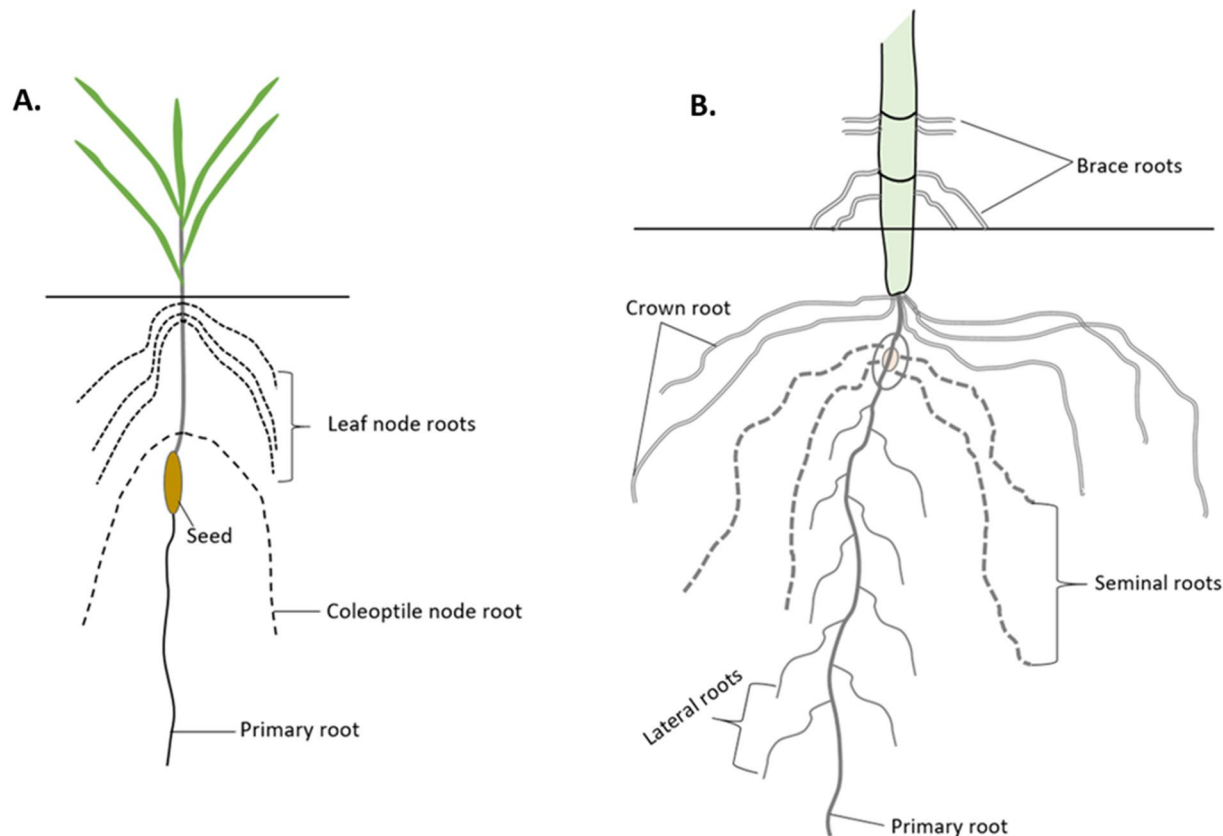
Figure A1. The root systems of (a) Brachypodium (*Brachypodium distachyon* L.) and (b) Maize (*Zea mays*) with the location of the primary roots investigated in this study.

A2. Maize Root System

Maize is an herbaceous monocot with an annual cycle (Alarcon et al., 2014). Its root system (Figure A1b) is categorized into embryonic and postembryonic roots (Feldman, 1994; Kiesselbach, 1999) based on the stage of formation. The embryonic roots of Maize consist of one primary root and several seminal roots (Hochholdinger, 2009), while the postembryonic roots of Maize consist of shoot-borne roots and lateral roots. The primary root is formed endogenously in the embryo (Yamashita, 1991), and it emerges from the base of the seed. The primary root is essential in the early stages of development. The primary roots may or may not remain functional during the life cycle of the plant. Some genotypes have active primary roots in their entire life cycle (Kausch, 1967; Kiesselbach, 1999), whereas other genotypes have primary roots that become inactive after the emergence of shoot-borne roots (Feldman, 1994).

Appendix B: Microscopic Sections of Maize Primary Roots From 8 to 29 DAS

Figure B1 shows that Aerenchyma first appeared in Maize primary roots at 8 DAS and remained till 29 DAS.
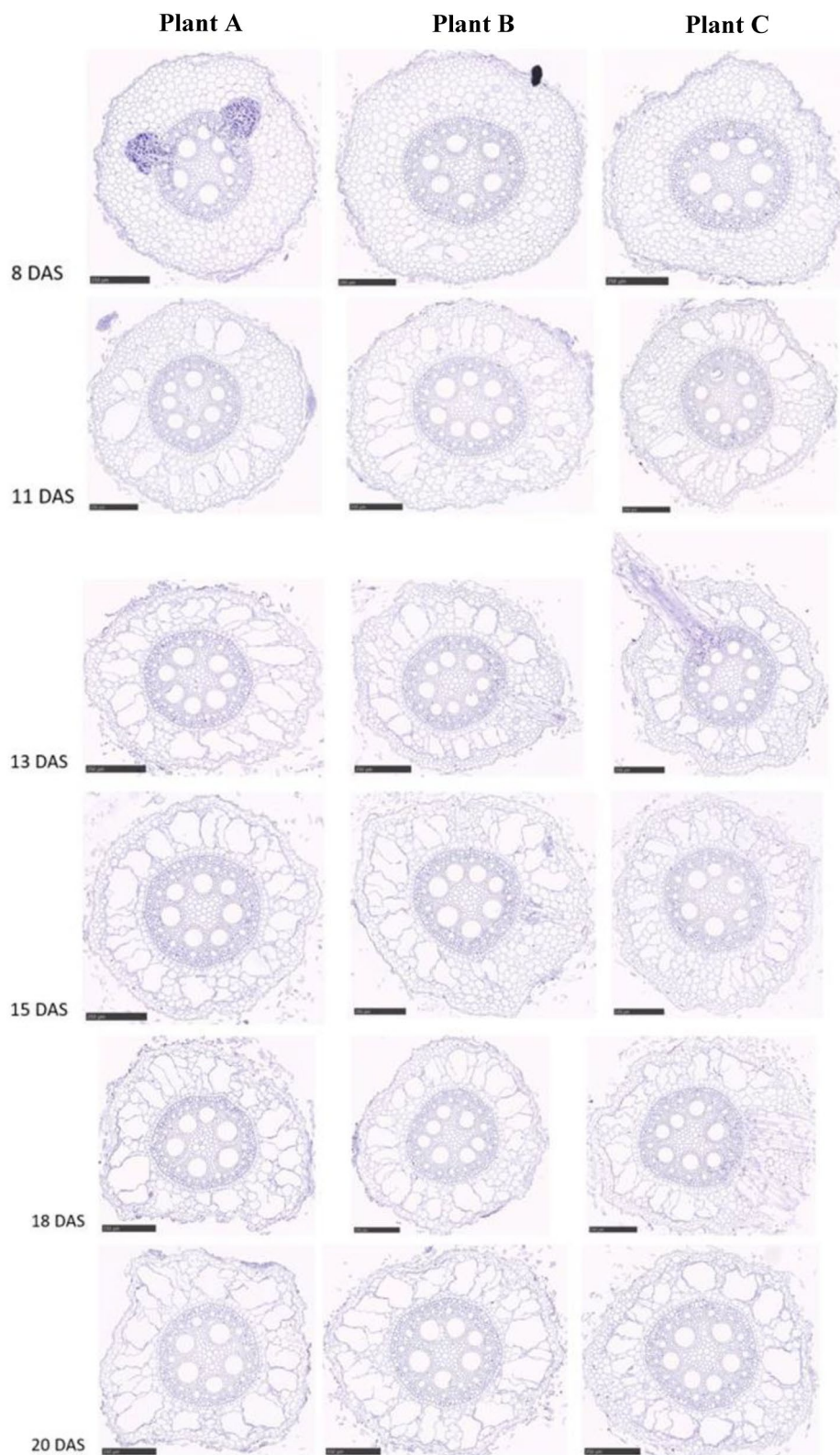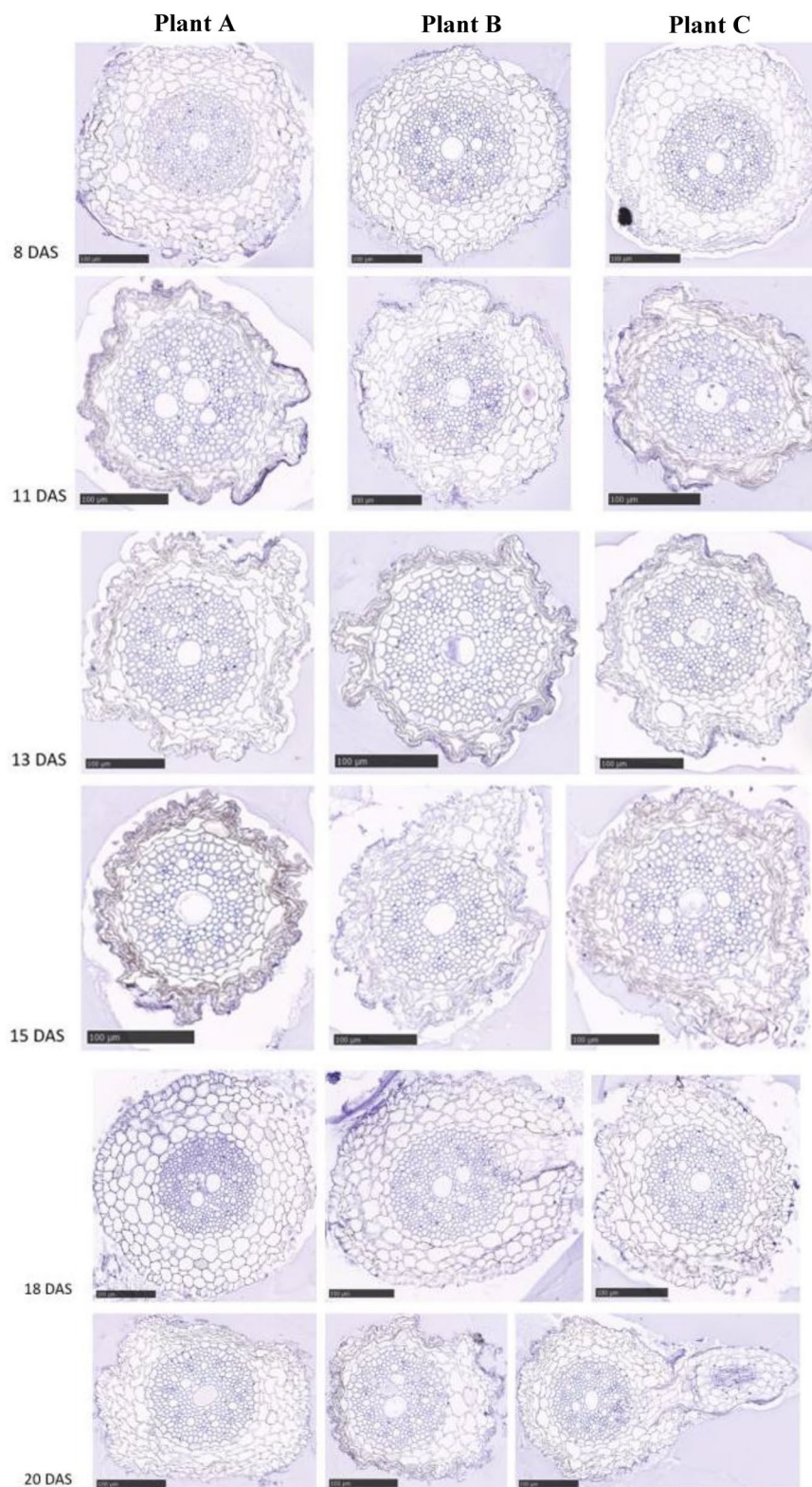
Figure B1. Microscopic sections of Maize primary roots showing the presence of Aerenchyma from 11–29 DAS.
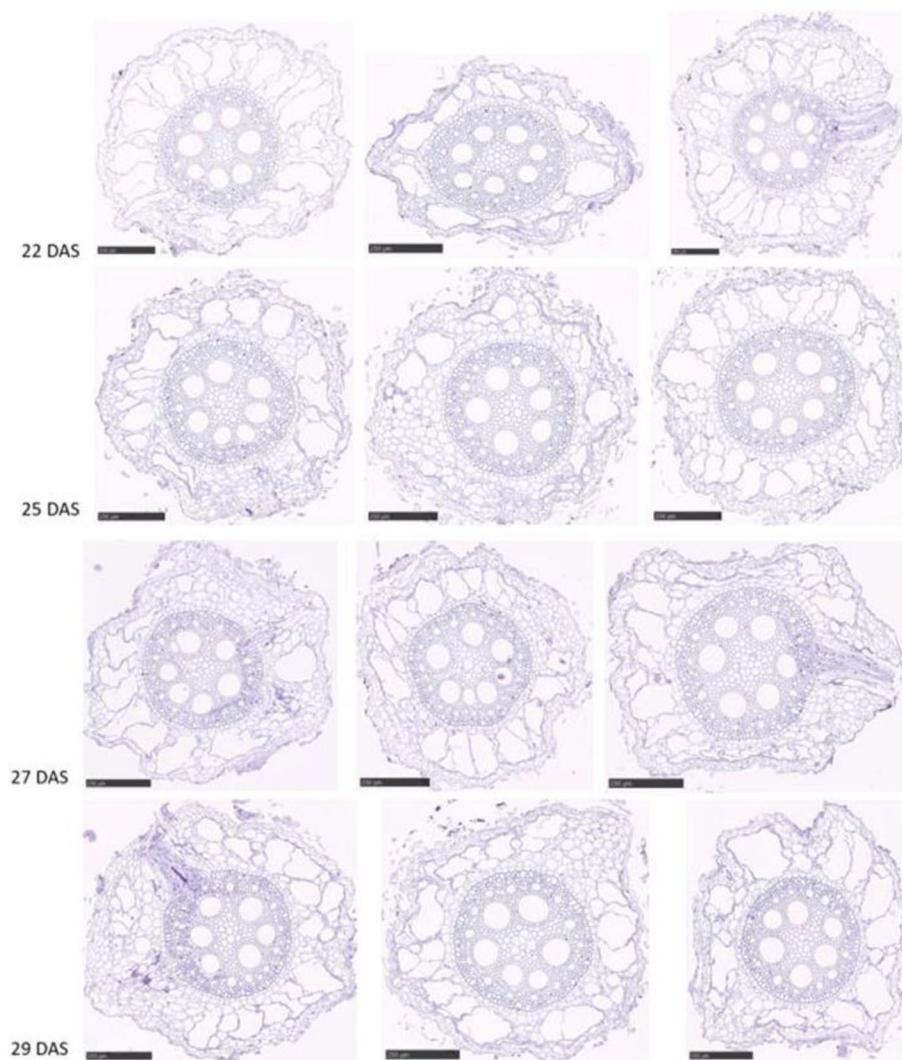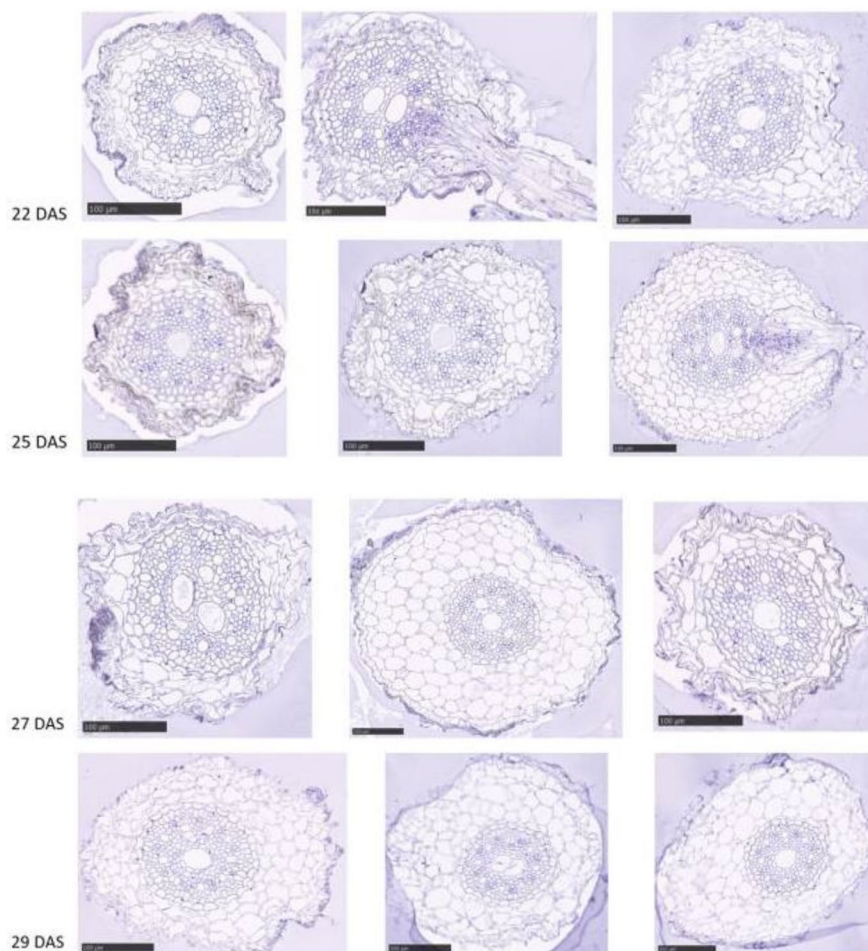
Figure B1. (Continued)

Appendix C: Microscopic Sections of Brachypodium Primary Roots From 8 to 29 DAS

Figure C1. Microscopic sections of Brachypodium primary roots showing visible shrinkage between 8 and 29 DAS.

Figure C1. (Continued)

Figure C1 shows that significant shrinkage occurred in Brachypodium primary roots between 8 and 29 DAS.

Data Availability Statement

Data associated with this study are available from the Mendeley data repository (Ehosioke et al., 2023).

References

Abdel Aal, G. Z., Atekwana, E. A., Slater, L. D., & Atekwana, E. A. (2004). Effects of microbial processes on electrolytic and interfacial electrical properties of unconsolidated sediments. *Geophysical Research Letters*, *31*, L12505. https://doi.org/10.1029/2004GL020030

Abdel Aal, G. Z., Slater, L. D., & Atekwana, E. A. (2006). Induced-polarization measurements on unconsolidated sediments from a site of active hydrocarbon biodegradation. *Geophysics*, *71*(2), H13–H24. https://doi.org/10.1190/1.2187760

Alarcón, M. V., Lloret, P. G., & Salguero, J. (2014). The development of the maize root system: Role of auxin and ethylene. In A. Morte, & A. Varma (Eds.), *Root engineering* (pp. 75–103). Springer. https://doi.org/10.1007/978-3-642-54276-3_5

Allred, B. J., Daniels, J. J., & Ehsani, M. R. (2008). *Agricultural geophysics*. CRC Press.

Amato, M., Basso, B., Cellano, G., Bitella, G., Morelli, G., & Rossi, R. (2008). In situ detection of tree root distribution and biomass by multielectrode resistivity imaging. *Tree Physiology*, *28*(8), 1441–1448. https://doi.org/10.1093/treephys/28.8.1441

Anderson, W. P., & Higinbotham, N. (1976). Electrical resistances of corn root segments. *Plant Physiology*, *57*(2), 137–141. https://doi.org/10.1104/pp.57.2.137

Atekwana, E. A., & Slater, L. D. (2009). Biogeophysics: A new Frontier in Earth science research. *Reviews of Geophysics*, *47*, RG4004. https://doi.org/10.1029/2009RG000285

Atekwana, E. A., Werkema, D. D., & Atekwana, E. A. (2006). Biogeophysics: The effects of microbial processes on geophysical properties of the shallow subsurface. In H. Vereecken, A. Binley, G. Cassiani, A. Revil, & K. Titov (Eds.), *Applied hydrogeophysics* (p. 383). Springer.

Atkinson, J. A., Pound, M. P., Bennett, M. J., & Wells, D. M. (2019). Uncovering the hidden half of plants using new advances in root phenotyping. *Current Opinion in Biotechnology*, *55*, 1–8. https://doi.org/10.1016/J.COPBIO.2018.06.002

Aubrecht, L., Zdenek, S., & Koller, J. (2006). Electrical measurement of the absorption surfaces of tree roots by the earth impedance method: 1. Theory. *Tree Physiology*, *26*(9), 1105–1112. https://doi.org/10.1093/treephys/26.9.1105

Barrowclough, D. E., Peterson, C. A., & Steudle, E. (2000). Radial hydraulic conductivity along developing onion roots. *Journal of Experimental Botany*, *51*(344), 547–557. https://doi.org/10.1093/jexbot/51.344.547

Beff, L., Günther, T., Vandoorne, B., Couvreur, V., & Javaux, M. (2013). Three-dimensional monitoring of soil water content in a maize field using electrical resistivity tomography. *Hydrology and Earth System Sciences*, *17*(2), 595–609. https://doi.org/10.5194/hess-17-595-2013

Bennett, M. J., Marchant, A., Green, H. G., May, S. T., Ward, S. P., Millner, P. A., et al. (1996). Arabidopsis AUX1 gene: A permease-like regulator of root gravitropism. *Science*, *273*(5277), 948–950. https://doi.org/10.1126/science.273.5277.948

Bera, T. K., Nagaraju, J., & Lubineau, G. (2016). Electrical impedance spectroscopy (EIS)-based evaluation of biological tissue phantoms to study multifrequency electrical impedance tomography (Mf-EIT) systems. *Journal of Visualization*, *19*(4), 691–713. https://doi.org/10.1007/s12650-016-0351-0

Binley, A., Slater, L. D., Fukes, M., & Cassiani, G. (2005). Relationship between spectral induced polarization and hydraulic properties of saturated and unsaturated sandstone. *Water Resources Research*, *41*, W12417. https://doi.org/10.1029/2005WR004202

Borner, F. D., Schopper, J. R., & Weller, A. (1996). Evaluation of transport and storage properties in the soil and groundwater zone from induced polarization measurements1. *Geophysical Prospecting*, *44*(4), 583–601. https://doi.org/10.1111/j.1365-2478.1996.tb00167.x

Bücker, M., & Hördt, A. (2013). Analytical modelling of membrane polarization with explicit parametrization of pore radii and the electrical double layer. *Geophysical Journal International*, *194*(2), 804–813. https://doi.org/10.1093/gji/ggt136

Cao, Y., Repo, T., Silvennoinen, R., Lehto, T., & Pelkonen, P. (2010). An appraisal of the electrical resistance method for assessing root surface area. *Journal of Experimental Botany*, *61*(9), 2491–2497. https://doi.org/10.1093/jxb/erq078

Chochois, V., Vogel, J. P., & Watt, M. (2012). Application of Brachypodium to the genetic improvement of wheat roots. *Journal of Experimental Botany*, *63*(9), 3467–3474. https://doi.org/10.1093/jxb/ers044

Chopin, J., Laga, H., Huang, C. Y., Heuer, S., & Miklavcic, S. J. (2015). RootAnalyzer: A cross-section image analysis tool for automated characterization of root cells and tissues. *PLoS One*, *10*(9), e0137655. https://doi.org/10.1371/journal.pone.0137655

Cseresnyés, I., Rajkai, K., Takacs, T., & Vozary, E. (2018). Electrical impedance phase angle as an indicator of plant root stress. *Biosystems Engineering*, *169*, 226–232. https://doi.org/10.1016/j.biosystemseng.2018.03.004

Cseresnyés, I., Takács, T., Végh, K. R., Anton, A., & Rajkai, K. (2013). Electrical impedance and capacitance method: A new approach for detection of functional aspects of arbuscular mycorrhizal colonization in maize. *European Journal of Soil Biology*, *54*, 25–31. https://doi.org/10.1016/j.ejsobi.2012.11.001

Dalton, F. N. (1995). In-situ root extent measurements by electrical capacitance methods. *Plant and Soil*, *173*(1), 157–165. https://doi.org/10.1007/BF00155527

Deacon, J. W., & Henry, C. M. (1978). Death of the cereal root cortex: Its relevance to biological control of take-all. *Annals of Applied Biology*, *89*(1), 100. https://doi.org/10.1111/j.1744-7348.1978.tb02576.x

Ehosioke, S., Garre, S., Huisman Johan, J. A., Zimmermann, E., Placencia-Gomez, E., Javaux, M., & Nguyen, F. (2023). *Complex electrical signatures of Maize and Brachypodium primary roots*. Mendeley Data, V1. https://doi.org/10.17632/g4g3zjb4sg.1

Ehosioke, S., Garre, S., Kremer, T., Rao, S., Kemna, A., Huisman, J. A., et al. (2018). A new method for characterizing the complex electrical properties of root segments. *Paper presented at the 10th Symposium of the International Society of Root Research, Ma'ale Hahamisha, Israel. 8–12 July 2018*.

Ehosioke, S., Nguyen, F., Rao, S., Kremer, T., Placencia-Gomez, E., Huisman, J. A., et al. (2020). Sensing the electrical properties of roots: A review. *Vadose Zone Journal*, *19*(1), e20082. https://doi.org/10.1002/vzj2.20082

Ehosioke, S., Phalempin, M., Garre, S., Kemna, A., Huisman, J. A., Javaux, M., & Nguyen, F. (2017). Developing suitable methods for effective characterization of electrical properties of root segments. In *Geophysical research abstracts* (Vol. 19). European Geosciences Union. Retrieved from http://hdl.handle.net/2268/213406

Ellis, T., Murray, W., & Kavalieris, L. (2013). Electrical capacitance of bean (*Vicia faba*) root systems was related to tissue density—A test for the Dalton model. *Plant and Soil*, *366*(1–2), 575–584. https://doi.org/10.1007/s11104-012-1424-z

Ernston, K., & Kirsch, R. (2006). Geoelectrical methods. In R. Kirsch (Ed.), *Groundwater geophysics* (2nd ed.). Springer.

Feldman, L. (1994). The maize root. In *The maize handbook* (pp. 29–37). Springer. https://doi.org/10.1007/978-1-4612-2694-9_4

Garré, S., Coteur, I., Wongleecharoen, C., Kongkaew, T., Diels, J., & Vanderborght, J. (2013). Noninvasive monitoring of soil water dynamics in mixed cropping systems: A case study in Ratchaburi Province, Thailand. *Vadose Zone Journal*, *12*(2), 1–12. https://doi.org/10.2136/vzj2012.0129

Garré, S., Javaux, M., Vanderborght, J., Pagès, L., & Vereecken, H. (2011). Three-dimensional electrical resistivity tomography to monitor root zone water dynamics. *Vadose Zone Journal*, *10*(1), 412–424. https://doi.org/10.2136/vzj2010.0079

Hardtke, C. S., & Pacheco-Villalobos, D. (2015). The *Brachypodium distachyon* root system: A tractable model to investigate grass roots. In J. Vogel (Ed.) *Genetics and genomics of Brachypodium. Plant genetics and genomics: Crops and models*, (Vol. 18, pp. 291–311). Springer. https://doi.org/10.1007/7397

Hille, B. (2001). *Ion channels of excitable membranes* (3rd ed.). Sinauer Associates, Inc.

Hochholdinger, F. (2009). The maize root system: Morphology, anatomy, and genetics. In J. L. Bennetzen, & S. C. Hake (Eds.), *Hand book of Maize, its biology* (pp. 145–160). Springer Science+Business Media LLC. https://doi.org/10.1007/978-0-387-79418-1

Huisman, J. A., Zimmermann, E., Esser, O., Haegel, F.-H., Treichel, A., & Vereecken, H. (2016). Evaluation of a novel correction procedure to remove electrode impedance effects from broadband SIP measurements. *Journal of Applied Geophysics*, *135*, 466–473. https://doi.org/10.1016/j.jappgeo.2015.11.008

Julien, J., Desbiez, M., de Jaegher, M., & Frachisse, J. (1991). Characteristics of the wave of depolarization induced by wounding in *Bidens pilosa* L. *Journal of Experimental Botany*, *42*(1), 131–137. https://doi.org/10.1093/jxb/42.1.131

Kao, K. C. (2004). *Dielectric phenomena in solids with emphasis on physical concepts of electronic processes*. Elsevier Academic Press.

Kausch, W. (1967). Lebensdauer der Primärwurzel von Monokotylen. *Naturwissenschaften*, *54*(17), 475. https://doi.org/10.1007/BF00684118

Kessouri, P., Furman, A., Huisman, J. A., Martin, T., Mellage, A., Ntarlagiannis, D., et al. (2019). Induced polarization applied to biogeophysics: Recent advances and future prospects. *Near Surface Geophysics*, *17*(6), 595–621. https://doi.org/10.1002/nsg.12072

Kiesselbach, T. A. (1999). *The structure and reproduction of corn. 50th Anniversary Edition*. Cold Spring Harbor Laboratory Press.

Kinraide, T. B. (2001). Ion fluxes considered in terms of membrane-surface electrical potentials. In *Australian Journal of Plant Physiology* (Vol. 28, pp. 605–616). CSIRO. https://doi.org/10.1071/pp00199

Kinraide, T. B., & Wang, P. (2010). The surface charge density of plant cell membranes (σ): An attempt to resolve conflicting values for intrinsic σ. *Journal of Experimental Botany*, *61*(9), 2507–2518. https://doi.org/10.1093/jxb/erq082

Kizhlo, M., & Kanbergs, A. (2009). *The causes of the parameters changes of soil resistivity* (pp. 43–46). Scientific Proceedings of Riga Technical University. https://doi.org/10.2478/v10144-009-0009-z

Li, M. Q., Li, J. Y., Wei, X. H., & Zhu, W. J. (2017). Early diagnosis and monitoring of nitrogen nutrition stress in tomato leaves using electrical impedance spectroscopy. *International Journal of Agricultural and Biological Engineering*, *10*(3), 194–205. https://doi.org/10.25165/IJABE.V10I3.3188

Liu, Y., Li, D. M., Qian, J., Di, B., Zhang, G., & Ren, Z. H. (2021). Electrical impedance spectroscopy (EIS) in plant roots research: A review. *Plant Methods*, *17*(1), 118. https://doi.org/10.1186/s13007-021-00817-3

Lynch, J. (1995). Root architecture and plant productivity. In *Plant physiology*. American Society of Plant Biologists. https://doi.org/10.1104/pp.109.1.7

Marchant, A., Kargul, J., May, S. T., Muller, P., Delbarre, A., Perrot-Rechenmann, C., & Bennett, M. J. (1999). AUX1 regulates root gravitropism in *Arabidopsis* by facilitating auxin uptake within root apical tissues. *EMBO Journal*, *18*(8), 2066–2073. https://doi.org/10.1093/emboj/18.8.2066

Martin, T. (2012). Complex resistivity measurements on oak. *European Journal of Wood and Wood Products*, *70*(1–3), 45–53. https://doi.org/10.1007/s00107-010-0493-z

Martin, T., Nordsiek, S., & Weller, A. (2015). Low-frequency impedance spectroscopy of wood. *Journal of Research in Spectroscopy*, *2015*, 910447. https://doi.org/10.5171/2015.910447

Mary, B., Abdulsamad, F., Saracco, G., Peyras, L., Vennetier, M., Mériaux, P., & Camerlynck, C. (2017). Improvement of coarse root detection using time and frequency induced polarization: From laboratory to field experiments. *Plant and Soil*, *417*(1–2), 243–259. https://doi.org/10.1007/s11104-017-3255-4

Mary, B., Saracco, G., Peyras, L., Vennetier, M., Mériaux, P., & Camerlynck, C. (2016). Mapping tree root system in dikes using induced polarization: Focus on the influence of soil water content. *Journal of Applied Geophysics*, *135*, 387–396. https://doi.org/10.1016/j.jappgeo.2016.05.005

Mathie, A., Kennard, L. E., & Veale, E. L. (2003). Neuronal ion channels and their sensitivity to extremely low frequency weak electric field effects. *Radiation Protection Dosimetry*, *106*(4), 311–315. https://doi.org/10.1093/oxfordjournals.rpd.a006365

Meunier, F., Zarebanadkouki, M., Ahmed, M. A., Carminati, A., Couvreur, V., & Javaux, M. (2018). Hydraulic conductivity of soil-grown lupine and maize unbranched roots and maize root-shoot junctions. *Journal of Plant Physiology*, *227*, 31–44. https://doi.org/10.1016/j.jplph.2017.12.019

Meyer, A. J., & Weisenseel, M. H. (1997). Wound-induced changes of membrane voltage, endogenous currents, and ion fluxes in primary roots of maize. *Plant Physiology*, *114*(3), 989–998. https://doi.org/10.1104/pp.114.3.989

Michot, D., Benderitter, Y., Dorigny, A., Nicoullaud, B., King, D., & Tabbagh, A. (2003). Spatial and temporal monitoring of soil water content with an irrigated corn crop cover using surface electrical resistivity tomography. *Water Resources Research*, *39*(5), 1138. https://doi.org/10.1029/2002WR001581

Miyazawa, Y., & Takahashi, H. (2020). Molecular mechanisms mediating root hydrotropism: What we have observed since the rediscovery of hydrotropism. *Journal of Plant Research*, *133*(1), 3–14. https://doi.org/10.1007/s10265-019-01153-3

Morrison, R. (1998). *Grounding and shielding techniques* (4th ed.). Wiley.

Paglis, C. M. (2013). Application of electrical resistivity tomography for detecting root biomass in coffee trees. *International Journal of Geophysics*, *2013*, 1–6. https://doi.org/10.1155/2013/383261

Poiré, R., Chochois, V., Sirault, X. R. R., Vogel, J. P., Watt, M., & Furbank, R. T. (2014). Digital imaging approaches for phenotyping whole plant nitrogen and phosphorus response in *Brachypodium distachyon*. *Journal of Integrative Plant Biology*, *56*(8), 781–796. https://doi.org/10.1111/jipb.12198

Repo, T., Cao, Y., Silvennoinen, R., & Ozier-Lafontaine, H. (2012). Electrical impedance spectroscopy and roots. In *Measuring roots* (pp. 25–49). Springer. https://doi.org/10.1007/978-3-642-22067-8_2

Roblin, G. (1985). Analysis of the variation potential induced by wounding in plants. *Plant and Cell Physiology*, *26*(3), 455–461. https://doi.org/10.1093/oxfordjournals.pcp.a076929

Rossi, R., Amato, M., Bitella, G., Bochicchio, R., Ferreira Gomes, J. J., Lovelli, S., et al. (2011). Electrical resistivity tomography as a non-destructive method for mapping root biomass in an orchard. *European Journal of Soil Science*, *62*(2), 206–215. https://doi.org/10.1111/j.1365-2389.2010.01329.x

Schleifer, N., Weller, A., Schneider, S., & Junge, A. (2002). Investigation of a Bronze Age plankway by spectral induced polarization. *Archaeological Prospection*, *9*(4), 243–253. https://doi.org/10.1002/arp.194

Schneider, H. M., & Lynch, J. P. (2018). Functional implications of root cortical senescence for soil resource capture. In *Plant and soil*. Springer International Publishing. https://doi.org/10.1007/s11104-017-3533-1

Schwan, H. P., & Takashima, S. (1991). Dielectric behavior of biological cells and membranes. *Bulletin of the Institute for Chemical Research, Kyoto University*, *69*, 459–475.

Slovak, R., Ogura, T., Satbhai, S. B., Ristova, D., & Busch, W. (2016). Genetic control of root growth: From genes to networks. *Annals of Botany*, *117*(1), 9–24. https://doi.org/10.1093/aob/mcv160

Srayeddin, I., & Doussan, C. (2009). Estimation of the spatial variability of root water uptake of maize and sorghum at the field scale by electrical resistivity tomography. *Plant and Soil*, *319*(1–2), 185–207. https://doi.org/10.1007/s11104-008-9860-5

Su, S. H., Gibbs, N. M., Jancewicz, A. L., & Masson, P. H. (2017). Molecular mechanisms of root gravitropism. *Current Biology*, *27*(17), R964–R972. https://doi.org/10.1016/j.cub.2017.07.015

Tsukanov, K., & Schwartz, N. (2020). Relationship between wheat root properties and its electrical signature using the spectral induced polarization method. *Vadose Zone Journal*, *19*, e20014. https://doi.org/10.1002/vzj2.20014

Wang, P., Kinraide, T. B., Zhou, D., Kopittke, P. M., & Peijnenburg, W. J. G. M. (2011). Plasma membrane surface potential: Dual effects upon ion uptake and toxicity. *Plant Physiology*, *155*(2), 808–820. https://doi.org/10.1104/pp.110.165985

Weigand, M., & Kemna, A. (2017). Multi-frequency electrical impedance tomography as a non-invasive tool to characterize and monitor crop root systems. *Biogeosciences*, *14*(4), 921–939. https://doi.org/10.5194/bg-14-921-2017

Weigand, M., & Kemna, A. (2019). Imaging and functional characterization of crop root systems using spectroscopic electrical impedance measurements. *Plant and Soil*, *435*(1–2), 201–224. https://doi.org/10.1007/s11104-018-3867-3

Yamashita, T. (1991). Ist die Primärwurzel bei Samenpflanzen exogen oder endogen? (Überlegungen zu Siegert's Buch "Zur Phylogenie der Wurzel"). *Beiträge Zur Biologie Der Pflanzen*, *66*, 371–391.

Zanetti, C., Weller, A., Vennetier, M., & Mériaux, P. (2011). Detection of buried tree root samples by using geoelectrical measurements: A laboratory experiment. *Plant and Soil*, *339*(1–2), 273–283. https://doi.org/10.1007/s11104-010-0574-0

Zimmermann, E., Kemna, A., Berwix, J., Glaas, W., Münch, H. M., & Huisman, J. A. (2008). A high-accuracy impedance spectrometer for measuring sediments with low polarizability. *Measurement Science and Technology*, *19*(10), 105603. https://doi.org/10.1088/0957-0233/19/10/105603